Sołtys *et al.*
Cell Communication and Signaling (2025) 23:243
https://doi.org/10.1186/s12964-025-02247-3

Cell Communication and Signaling

RESEARCH

Open Access

The intrinsically disordered AB region: a key modulator of the molecular properties of human RXRγ

Katarzyna Sołtys[1*], Krzysztof Skowronek[2], Dominika Bystranowska[1], Krzysztof Wycisk[2] and Andrzej Ożyhar[1]

Abstract

The human retinoid X receptor γ (*h*RXRγ) is one of three characterized RXR subtypes, transcription factors belonging to the nuclear receptor superfamily. All RXR subtypes share nearly identical structural elements, including a conserved DNA-binding domain, a D region, a ligand-binding domain, and an F region. However, each subtype possesses a unique N-terminal AB region, which modulates the transcriptional activation of target genes in a cell- and promoter-dependent manner through its ligand-independent activation function involved in protein–protein interactions. Despite the functional significance of the AB region, its structural contributions, particularly in the context of the full-length receptor, remain largely unexplored. Here, we uncover the role of the AB region of *h*RXRγ in modulating the molecular properties of the receptor. A comparative analysis of the full-length receptor (*h*RXRγ) and a deletion mutant lacking the AB region (ΔAB*h*RXRγ) highlights the critical role of the intrinsically disordered AB region in modulating the structural and functional properties of *h*RXRγ, including its ability to oligomerize, its overall stability, and conformation heterogeneity. The AB region does not act as an independent unit but amalgamates with the rest of the receptor, which fine-tunes the structural variability of *h*RXRγ, making it responsive to environmental conditions. These findings highlight the AB region as a critical determinant of *h*RXRγ's structural features and, potentially, its transcriptional potential.

Keywords Nuclear receptors, Retinoid X receptor, Oligomerization, 9*c*RA, Stability, Intrinsically disordered regions

Background

The structural uniqueness of proteins largely determines their biological function. Intrinsically disordered proteins (IDPs) and intrinsically disordered regions (IDRs), unlike structured proteins, lack a fixed three-dimensional conformation under physiological conditions and instead exist as dynamic ensembles of conformations [1–4]. IDRs are abundant in nature and are important constituents of many proteins. IDRs, along with IDPs, play various structural, functional and regulatory roles [1, 5]. The unique physicochemical properties of IDPs/IDRs, particularly structural flexibility and ability to adopt multiple conformations, enable a single regulatory protein to interact with a variety of binding partners [6]. The multivalent interactions and the dynamic nature of IDPs/IDRs are key in driving phase separation which can lead to the formation of various membraneless organelles (MLOs) [7, 8]. Additionally, their conformational ensembles, and consequently their functional output, can be finely regulated by post-translational modifications [9]. Although IDPs/IDRs lack a signature sequence motif, they can be predicted based on their unique amino acid composition

*Correspondence:
Katarzyna Sołtys
katarzyna.soltys@pwr.edu.pl
[1] Department of Biochemistry, Molecular Biology and Biotechnology, Faculty of Chemistry, Wrocław University of Science and Technology, Wybrzeże Wyspiańskiego 27, Wrocław 50-370, Poland
[2] International Institute of Molecular and Cell Biology, 4 Ks. Trojdena Street, Warsaw 02-109, Poland

[10]. It has been observed that transcription factors (TFs) are often enriched with IDRs [11–15]. This enrichment suggests that IDRs play an important role in TF-dependent gene expression regulation.

Retinoid X receptor (RXR) is a ligand-dependent transcription regulator that belongs to the nuclear receptor (NR) superfamily. As a TF modulated by lipophilic molecules, RXR controls expression of targets genes involved in diverse physiological processes, including regulation of development, differentiation and metabolism [16]. RXR is an interacting partner for one-third of the 48 members of the human nuclear receptor superfamily including peroxisome proliferator-activated receptor (PPAR), retinoic acid receptor (RAR), vitamin D receptor (VDR), thyroid hormone receptor (TR), liver X receptor (LXR), farnesoid X receptor (FXR), and pregnane X receptor (PXR) [17]. Additionally, RXR regulates target gene expression as a homodimer and probably also as a homotetramer [18]. Given the wide variety of processes controlled by RXR, its dysregulation can contribute to numerous disease, including neurodegenerative disorders, obesity, diabetes and also cancer [19, 20].

RXR shares a conserved structural organization with other NRs, comprising five regions labelled A through F (Fig. 1A) [21]. The structural and functional similarities allow the distinction of two folded domains—the DNA-binding domain (DBD) and the ligand-binding domain (LBD)—which are surrounded by IDRs. DBD participates in the formation of receptor dimers with either itself (homodimer) or other NR (heterodimer) and guides the receptor to specific DNA sequences called hormone response elements (HREs). Most of the typical HREs for dimers containing RXR are direct repeats (DRs) that contain two hexa-nucleotide motifs A/GGGTCA separated with one to five nucleotide spacing (DR1-DR5) [22, 23]. DBD is separated from LBD by an intrinsically disordered hinge region (region D) (Fig. 1A). The flexibility of this region allows rotation of both domains and adaptation to variations in spacer lengths, facilitating DBD and LBD dimerization [24]. LBD is the most extensively studied fragment of RXRs. It mediates ligand binding, modulates oligomeric state of RXR and is important for activation of gene transcription as it contains ligand-dependent transactivation function (AF2). In the absence of ligand, RXR binds co-repressors that inhibit its transcriptional activity. It is also believed that RXR may self-associate and form transcriptionally inactive homotetramers [18, 25–27]. The function of these higher-order oligomers of RXR is not completely understood. The homotetramers could serve as a reservoir for the receptor [18, 25, 26] or they could function as structural elements capable of folding the DNA to bring distant HREs into close physical proximity [28]. Upon natural (e.g., 9-*cis*-retinoic acid, 9*c*RA) or synthetic ligands binding, RXR homotetramers dissociate, leading to homo- and heterodimers formation [29]. The presence of ligand also allows exchange co-repressor complexes to co-activator complexes, what stimulates transcription activity [30].

RXR is expressed in multiple variants, including three subtypes – RXRα, RXRβ and RXRγ – each of which can give rise to different isoforms [31]. The major differences among the subtypes lie within the AB regions, which are located at N-terminus of RXR (Fig. 1A). The AB regions contain an autonomous ligand-independent activation function (AF1) and are involved in multivalent protein–protein interactions, which are essential for modulating the transcriptional activation of target genes in a tissue-specific, as well as time-, stimuli- and promoter-dependent manner [32]. Importantly, the functional diversity of AB regions is not solely a consequence of their distinct sequences but also arises from their intrinsically disordered nature. This structural characteristic enables the AB regions to adopt multiple conformations, facilitating dynamic interactions with diverse binding partners and broadening their regulatory potential in transcription. Additionally, the unique properties of the AB regions may influence the ability to form higher-order oligomers, as subtype RXRβ, unlike RXRα and RXRγ, cannot form homotetramers [18]. Despite years of structural analysis of RXR, research has predominantly focused on RXRα, leaving a gap in the understanding of the other subtypes. Furthermore, numerous studies have concentrated on isolated regions or domains, primarily due to the difficulties associated with obtaining the full-length protein. Recent studies have described the biochemical and biophysical properties of the AB region in RXRγ [33, 34]. However, the complex structure–function relationship of the full-length RXRγ remains largely unexplored.

In this study, we successfully developed a protocol for the expression and purification of the full-length human retinoid X receptor γ (*h*RXRγ), enabling detailed investigation of its molecular properties in comparison to a deletion mutant lacking the AB region (ΔAB*h*RXRγ). Through hydrogen–deuterium exchange coupled with mass spectrometry, we demonstrated that the AB region of *h*RXRγ, within the context of the full-length protein, is intrinsically disordered. Biophysical characterization revealed that recombinant *h*RXRγ forms homodimers and higher-order oligomers. In contrast, the absence of the intrinsically disordered AB region significantly altered the molecular properties of the receptor molecule, particularly by reducing its tendency to form stable higher-order oligomers. Additionally, the AB region modulates the receptor's stability, as evidenced by the greater resistance of ΔAB*h*RXRγ to elevated temperatures and proteolytic digestion.

Furthermore, we demonstrate a direct interaction between the AB region and ΔAB*h*RXRγ, likely involving other structural domains of RXR, including the globular DBD and LBD. This interaction underscores the coordinated interplay between the AB region and other structural elements in modulating the receptor's molecular properties and conformational heterogeneity. Collectively, our results emphasize the critical role of the intrinsically disordered AB region in modulating the conformational states of the *h*RXRγ molecule, which fine-tune the receptor's molecular and, consequently, functional properties.

Methods

Chemicals

All buffers were prepared at room temperature. The lysis buffer contained 30 mM HEPES, 150 mM NaCl, pH 7.0. The buffer A contained 30 mM HEPES, 500 mM NaCl, 5% (v/v) glycerol, 1 mM DTT, pH 7.0. The buffer AB contained 30 mM HEPES, 500 mM NaCl, 5% (v/v) glycerol, 15 mM imidazole, 1 mM DTT, pH 7.0. The buffer B_FL contained 30 mM HEPES, 500 mM NaCl, 5% (v/v) glycerol, 500 mM imidazole, 1 mM DTT, pH 7.0. The buffer B_dAB contained 30 mM HEPES, 500 mM NaCl, 5% (v/v) glycerol, 500 mM imidazole, 1 mM DTT, pH 7.8. The buffer SEC300_FL contained 30 mM HEPES, 300 mM NaCl, 5% (v/v) glycerol, 1 mM DTT, pH 7.0. The buffer SEC300_dAB contained 30 mM HEPES, 300 mM NaCl, 5% (v/v) glycerol, 1 mM DTT, pH 7.8. The buffer AUC_FL contained 30 mM HEPES, 300 mM NaCl, 2%(v/v) glycerol, pH 7.0. The buffer AUC_dAB contained 30 mM HEPES, 300 mM NaCl, 2%(v/v) glycerol, pH 7.8. The buffer D_50, buffer D_150 and buffer D_300 contained 30 mM HEPES, 50/150/300 mM NaCl, 2% (v/v) glycerol, pH 7.0 (FL)/7.8 (dAB). MST assay buffer (30 mM HEPES, 200 mM NaCl, 5% (v/v) glycerol, 0.05% Tween 20, pH 7.0). RXR ligand – 9-*cis*-retinoic acid (9cRA) was purchased from Sigma-Aldrich (R4643).

Preparation of the cDNA constructs

The *E. coli* strain DH5α (Thermo Fisher Scientific) was used as the host strain for the cloning procedures. The sequence of the full-length human RXRγ (*h*RXRγ) was taken from UniProtKB—P48443. The cDNA of *h*RXRγ was de novo synthetized in GeneArt® (Thermo Fisher Scientific). The gene sequence was optimized using Gene Optimizer software to maximize the expression of the synthetic gene in *E. coli*. An optimized sequence was used as the template for PCR to obtain the full-length RXRγ (*h*RXRγ) and the deletion mutant that lacks the AB region (ΔAB*h*RXRγ). The following primers were used for the amplification of *h*RXRγ – forward: GCGCGG CCATGGGAtatggcaactatagccac; reverse: GCGCGG GCGGCCGCttaggtaatctgcagcggagtttc, and for the amplification of ΔAB*h*RXRγ – forward: GCGCGGCCATGG GAagcaccagtccgggtagcc; reverse: GCGCGC GCGGCC GCttaggtaatctgcagcggag. The forward primers introduced the *Nco*I, and the reverse primers the *Not*I restriction sites. The capital letters in the sequences represent nucleotides that are added to the coding sequences for cloning purposes, whereas the restriction sites are underlined. The inserts were ligated with the pETHSu plasmid in a frame with the sequence that encodes the N-terminal peptide containing the polyhistidine (6 ×His) tag and SUMO [35]. The sequence of the obtained construct was verified by DNA sequencing.

Expression and purification of the proteins

The *h*RXRγ and ΔAB*h*RXRγ were expressed in the *E. coli* strain ArcticExpress (DE3) (Agilent). Bacterial cells harboring the expression vector were grown in ZYM-5052 auto-inducing media [36] supplemented with 50 μg/ml kanamycin. The culture was grown at 37 °C and 182 rpm until an optical density (OD_{600}) reached the value of 1.0 and thereafter protein was expressed at 15 °C overnight. The cells were harvested by centrifugation at 5,000 ×g at 4 °C for 15 min. The pellet of bacteria was suspended in ice-cold lysis buffer containing PMSF (0.2 mg/ml) and lysozyme (1 mg/ml), then stored at − 80 °C until use.

The frozen cell suspension supplemented with DNase (20 μg/ml), RNase (20 μg/ml) and a fresh portion of PMSF (0.2 mg/ml) was slowly thawed at 10 °C. The cell lysis was improved by sonication. The cell suspension was sonicated with 5 short bursts of 20 s, followed by intervals of 30 s for cooling. The resulting suspension was centrifuged at 18,000 ×g at 4 °C for 1 h. The soluble fractions containing *h*RXRγ and ΔAB*h*RXRγ supplemented with PMSF (0.2 mg/ml) were purified using immobilized metal affinity chromatography (IMAC). The cell lysate was incubated for 1 h at 10 °C with Talon® Metal Affinity Resin (Clontech), which had been previously equilibrated with lysis buffer. The resin was washed with buffer A and AB until the absorbance at 280 nm was lower than 0.1. Next the resin was equilibrated with buffer SEC300_FL or SEC300_dAB during purification of *h*RXRγ or ΔAB*h*RXRγ, respectively. 0.5 mg SUMO hydrolase (dtUD1) [37] was added to the resin, gently mixed and incubated overnight at 4 °C. After overnight digestion the resin was washed with buffer SEC300_FL or SEC300_dAB. Only a small amount of *h*RXRγ and ΔAB*h*RXRγ were present in these fractions, as both proteins bind to the resin after digestion with dtUD1. *h*RXRγ and ΔAB*h*RXRγ were eluted with buffer B_FL or B_dAB, and next

concentrated to a total volume of 500 µl using the Amicon Ultracel-4 Centrifugal Filter Units (Merck Millipore) with a cut-off limit of 30 kDa. Both proteins were purified to homogeneity using Superdex 200 Increase 10/300 GL column (GE Healthcare Life Sciences) pre-equilibrated with buffer SEC300_FL or SEC300_dAB and connected to an ÄKTA Avant system (GE Healthcare Life Sciences). The purification was performed at a 0.5 ml/min flow rate at room temperature. Fractions containing the purified *h*RXRγ or ΔAB*h*RXRγ were combined and concentrated to 1 mg/ml using the Amicon Ultracel-4 Centrifugal Filter Units (Merck Millipore) with a cut-off limit of 30 kDa and then aliquoted into small volumes. These preparations were used for subsequent experiments unless otherwise stated. The concentration of *h*RXRγ and ΔAB*h*RXRγ was determined spectrophotometrically at 280 nm. The absorption coefficients calculated according to Gill and von Hippel [38], were 0.655 ml/(mg × cm) for *h*RXRγ and 0.637 ml/(mg × cm) for ΔAB*h*RXRγ. The samples were stored at − 80 °C. The molecular mass of *h*RXRγ and ΔAB*h*RXRγ were confirmed by ESI-TOF mass spectroscopy (Mass Spectrometry laboratory, IBB PAS, Warsaw). It was found to be 50 924 Da and 38 290 Da for *h*RXRγ and ΔAB*h*RXRγ, respectively. Both experimental values were in good agreement with the values of theoretical mass estimated with the ProtParam tool (50 928 Da and 38 291 Da for *h*RXRγ and ΔAB*h*RXRγ, respectively). All of the presented experiments in this paper were performed using samples obtained from several independent preparations. The results were reproducible and we did not observe any variability from different preparations.

Sodium dodecyl sulfate–polyacrylamide gel electrophoresis (SDS-PAGE)

The protein samples were analyzed by SDS-PAGE using 4%/12% or 4%/15% polyacrylamide gels [39]. Electrophoresis was performed at a constant current 20 mA/1 mm gel. The Unstained Protein Molecular Weight Marker was used (Thermo Fisher Scientific). After electrophoresis, the gels were stained with Coomassie Brilliant Blue R-250 [40] and analyzed using Image Lab Software (Bio-Rad).

Size-exclusion chromatography with multi-angle light scattering (SEC-MALS)

SEC-MALS was performed using a ÄKTA Purifier chromatography system equipped with a UV detector. Samples were monitored at a wavelength of 280 nm. The chromatography system was connected to in-line detectors: a MALS detector (DAWN 8+) and a differential refractometer (Optilab T-rEX). Samples for SEC-MALS were prepared during purification by separating *h*RXRγ and ΔAB*h*RXRγ fractions into two categories: *h*RXRγ_oligomer and ΔAB*h*RXRγ_oligomer (first peak, smaller elution volume), and *h*RXRγ_dimer and ΔAB*h*RXRγ _dimer (second peak, larger elution volume) (**Fig. S1** and **Fig. S2**). 100 µl of protein samples (5 mg/ml) were loaded onto a Superdex 200 Increase 10/300 column (GE Healthcare) equilibrated with buffer SEC300_FL or SEC300_dAB. Samples were run at room temperature at a flow rate of 0.75 ml/min. The results were analyzed using Astra 6 software in accordance with manufacturer's instructions.

Sedimentation velocity analytical ultracentrifugation experiments (SV-AUC)

Sedimentation velocity experiments were performed at 20 °C on a Beckman Coulter ProteomeLab XL-I ultracentrifuge (Beckman Coulter Inc.) in an An-60 Ti rotor. The samples for the SV-AUC experiment were prepared in the same manner as those for SEC-MALS. During purification, *h*RXRγ and ΔAB*h*RXRγ fractions were separated into two categories: *h*RXRγ_oligomer and ΔAB*h*RXRγ_oligomer (first peak, smaller elution volume) and *h*RXRγ_dimer and ΔAB*h*RXRγ _dimer (second peak, larger elution volume) (Fig. S1 and Fig. S2). Each protein sample (400 µl at three concentrations: 0.2 mg/ml, 0.4 mg/ml, or 0.8 mg/ml in buffer AUC) was loaded into two-channel centerpieces and centrifuged overnight at 35 000 rpm. Detection of the protein concentration was performed using OD measurements at a wavelength of 280 nm. The data were analyzed with SEDFIT software using a continuous size distribution *c*(s) model to extract the sedimentation coefficient (s) [41, 42]. The partial specific volumes (V_{bar}) of *h*RXRγ and ΔAB*h*RXRγ (0.733955 ml/g and 0.735667 ml/g respectively) and the density (1.0171 g/ml) and dynamic viscosity (0,019 mPa × s) of the buffer at 20 °C were calculated using SEDNTERP software [43]. Maximum entropy regularization with $p = 0.68$ was applied. The sedimentation coefficient (s), after correction for solvent density and viscosity in relation to the density and viscosity of water at 20 °C, were expressed as $s_{20,w}$. The hydrodynamic dimensions of *h*RXRγ and ΔAB*h*RXRγ were calculated by SEDFIT. The quality of the fits was assessed using RMSD values, residual distributions and residual histograms.

Hydrogen–deuterium exchange coupled with mass spectrometry (HDX-MS)

Hydrogen–deuterium exchange (HDX) experiments were performed using HDX Manager with on-line digestion and separation using a nanoACQUITY UPLC

System with HDX technology coupled to a SYNAPT G2 HDMS instrument (Waters). Initially, a non-deuterated sample was prepared by mixing 15 µl of the *h*RXRγ protein stock (40 µM) with 35 µl of buffer SEC300_FL, prepared in H_2O. The sample was then acidified with 10 µl of 2 M glycine–HCl and 4 M Gdm-HCl (pH 2.5) and digested on-line on an immobilized pepsin column (Poroszyme immobilized pepsin, ABI) with 0.07% formic acid in water as the mobile phase (flow rate, 200 µl/min). The resulting peptides were captured on a 2.1 × 5 mm C18 trap column (ACQUITY BEH C18 VanGuard pre-column, 1.7 µm resin; Waters) and then directly passed onto an ACQUITY UPLC-BEH C18 reversed-phase column (2.1 × 50 mm, 1.7 µm; Waters) and eluted using a gradient of 10%–35% acetonitrile in 0.1% (v/v) formic acid at a flow rate of 90 µl/min. The Manager system (Waters) was used to strictly maintain the temperatures of all fluids, valves, and columns at 0.5 °C, except for the pepsin column, which was maintained at 20 °C inside the temperature-controlled digestion compartment. For protein identification, mass spectra were acquired in MSE mode over an m/z range of 50–1950. The spectrometer parameters were as follows: ESI in positive mode; capillary voltage, 3 kV; sampling cone voltage, 35 V; extraction cone voltage, 3 V; source temperature, 80 °C; desolvation temperature, 175 °C; and desolvation gas flow, 800 l/h.

For deuterated samples, 5 µl of protein stock was diluted tenfold with 45 µl of buffer SEC300_FL, prepared in D_2O. The exchange reaction was performed for 10 s, 1 min, 5 min, 25 min or 120 min and then immediately quenched in 2 M glycine–HCl and 4 M Gdm-HCl (pH 2.5) cooled on ice. The samples were analyzed the same way as the non-deuterated sample, but the C18 column outlet was coupled directly to the ion source of the spectrometer, which, additionally, was run in ion mobility mode. Each experiment was carried out in triplicate.

Two control HDX-MS experiments were performed to account for minimum and maximum exchange of peptides. To obtain minimum exchange, D_2O reaction buffer was added to the quenching buffer cooled on ice prior to the addition of protein stock. For maximum exchange, 5 µl of protein stock was mixed with 45 µl of D_2O reaction buffer, incubated overnight, and then mixed with quenching buffer and analyzed as described above.

HDX-MS data analysis

Peptides were identified using ProteinLynx Global SERVER software (PLGS, Waters). The list of identified peptides was analyzed by the DynamX 3.0 program (Waters) with the following acceptance criteria: minimum intensity threshold of 3000 and minimum products per amino acid of 0.3. The isotopic envelopes of the peptides after exchange were analyzed using DynamX 3.0 with manual corrections wherever necessary. Percent sample deuteration was calculated with a formula that takes into consideration the molecular weights from the minimum ($M_{ex}0$) and maximum exchange ($M_{ex}100$) values of a given peptide:

$$D(\%) = \frac{(M_{ex} - M_{ex}0)}{(M_{ex}100 - M_{ex}0)} \times 100\%$$

Error bars for percent deuteration D (%) were calculated as standard deviations of three independent experiments. Final graphs were plotted using OriginLab 8.5.

Circular dichroism spectroscopy (CD)

Circular dichroism (CD) spectra were recorded using the Jasco-815 spectropolarimeter (Jasco Inc) equipped with the Peltier temperature controller (CDF-426S/15). The spectra were collected in a spectral range of 200–260 nm with a scanning speed of 50 nm/min, at 20 °C, D.I.T – 2 s and a 1 nm band width. The data pitch was 0.5 nm and the final spectrum was obtained after averaging three measurements. The spectra were measured using quartz cuvettes with a path length of 1 mm. The concentration of the full-length *h*RXRγ, ΔAB*h*RXRγ and the AB region were 10 µM (0.51 mg/ml, 0.38 mg/ml and 0.14 mg/ml, respectively). All spectra were recorded in 30 mM HEPES buffer containing 300 mM NaCl, 5% (v/v) glycerol and 1 mM DTT. For thermal-induced protein denaturation spectra were collected at temperatures ranging from 25 °C to 65 °C. The data pitch was 5 °C and the temperature gradient was 5 °C/min. Temperature-dependent denaturation was monitored by following the changes in ellipticity at 222 nm by increasing the temperature from 25 °C to 60 °C at a constant rate of 1 °C/min.

All the spectra were corrected for the effect from the buffer and converted to molar residual ellipticity units. The molar molecular mass per residue (MRW) for the full-length *h*RXRγ, ΔAB*h*RXRγ and the AB region are 110.0 Da, 113.6 Da and 102.9 Da respectively. Evaluation of the secondary structure content was calculated with CDPro deconvolution software using three algorithms: Continll, Selon3 and Cdsstr. IBasis 4 (SPD42) was used as the reference protein data set [44].

Fluorescence spectroscopy

8-anilino-1-naphthalenesulfonic acid (ANS) fluorescence measurements were performed on a Fluorolog-3 spectrofluorometer (Horiba Jobin Yvon Inc.) at 20 °C. The concentration of the ANS stock solutions was calculated using $\varepsilon_{351} = 6240\ M^{-1} \times cm^{-1}$ [45]. The protein

samples (*h*RXRγ and ΔAB*h*RXRγ) of 2 µM containing 20 µM ANS were prepared in buffers: SEC50_FL, SEC300_FL, SEC50_dAB or SEC300_dAB. ANS fluorescence was excited at 351 nm and the emission spectra were recorded at the wavelength range of 400–650 nm. The integration time of 0.5 s, and slits with bandwidths of 4 nm, were used. Measurements were performed in a 0.3 cm path-length quartz cuvette (105–251-15–40, Hellma).

Limited proteolysis

The 0.5 mg/ml purified the full-length *h*RXRγ and ΔAB*h*RXRγ were digested with endoproteinase Glu-C (V8) (Sigma-Aldrich) using a 1:250 (w/w) substrate-to-protease ratio. The control reactions did not contain enzyme. The proteolysis reactions were conducted at 25 °C in buffer D_50 and buffer D_300. The reactions in the presence of the RXR hormone response element, *Ramp2* DR1 DNA (1:2) and the RXR ligand, 9-*cis*-retinoic acid (1:8), were conducted in buffer D_150. After defined time intervals (0, 5, 15, 40, 75, 120 and 240 min), samples of 10 µl were taken, mixed with the 3 µl SDS loading buffer and heated for 10 min at 95 °C. Cleaved peptides were resolved using 15% SDS–polyacrylamide gels.

Microscale thermophoresis (MST)

The purified recombinant N-terminally 6× His-tagged AB region of *h*RXRγ [33] was labeled using a protein-labeling kit – His-Tag Labeling Kit RED-tris-NTA 2nd Generation (cat# MO-L018, NanoTemper Technologies) according to the manufacturer's instructions. The ligand, ΔAB*h*RXRγ, was prepared at a concentration of 280 µM (13 mg/ml), then serially diluted in MST assay buffer (30 mM HEPES, 200 mM NaCl, 5%(v/v) glycerol, 0.05% Tween 20, pH 7.0) and mixed with the labeled protein target to a final volume of 30 µl. The final target concentration was 50 nM. The samples were incubated at room temperature for 30 min and then loaded into MST premium coated capillaries (NanoTemper Technologies). The samples were analyzed on a MonolithX (MM-314) MST Instrument (NanoTemper Technologies, excitation power 100%, medium MST power). Data was processed with MO.Affinity.Analysis (NanoTemper). Binding constants were determined using a K_d model (details about the fitting model are available at the NanoTemper Technologies support page: https://support.nanotempertech.com/hc/en-us/articles/19206980835345).

Sequence analysis

Analysis of the *h*RXRγ sequence was performed using bioinformatics tools with default settings. The ProtParam tool (https://web.expasy.org/protparam/) allows the computation of various physical and chemical parameters (e.g. molecular mass, theoretical pI, extinction coefficient) [46]. The prediction of disorder regions was made using IUPred2 A (https://iupred2a.elte.hu/) [47, 48], PONDR (http://www.pondr.com) [11] and MetaDisorderMD2 (https://genesilico.pl/metadisorder/) [49] predictors. Protein backbone dynamics were predicted using DynaMine (http://dynamine.ibsquare.be) [50, 51]. The prediction of potential sites cleaved by endoproteinase Glu-C (V8) in *h*RXRγ sequence was made using a PeptideCutter (https://web.expasy.org/ peptide_cutter/) [46]. Structural model was generated using AlphaFold3 [52] and visualized with UCSF ChimeraX [53].

Results

Intrinsically disordered properties of the RXR sequence revealed by in silico analysis and hydrogen–deuterium exchange coupled with mass spectrometry

The amino acid sequence of the full-length *h*RXRγ was analyzed to evaluate the disorder propensity of the protein. To predict the presence of IDRs, three independent predictors were applied: IUPred2 [47, 48], PONDR [11] and MetaDisorderMD2 [49]. The results obtained with all the algorithms are largely consistent. As seen in Fig. 1B, *h*RXRγ appears to be composed of both ordered and unordered regions. The highest propensity for ordered structure is observed for DBD and LBD of *h*RXRγ. There are two major segments that were predicted to be disordered in *h*RXRγ, spanning: 1–130 and 180–260 amino acid residues (Fig. 1B). These fragments correspond to the AB region and D region of *h*RXRγ, respectively (Fig. 1A). In total, approximately 50% of the analyzed sequence was predicted to be disordered.

Additional in silico analysis was conducted using DynaMine algorithm, a tool that is designated for the prediction of protein backbone dynamics [50]. Values above 0.8 indicate an ordered state (rigid regions), whereas values below 0.69 indicate a disordered state (flexible regions) [51]. Obtained results for DynaMine algorithms are in good agreement with IUPred2, PONDR and MetaDisorderMD2 predictions. In total, approximately 50% of the analyzed sequence was predicted to be ordered. DynaMine identified also three highly flexible regions in *h*RXRγ (approximately 25% of the analyzed sequence), spanning: 1–130, 220–233 and 460–464 amino acid residues (Fig. 1C), corresponding to the AB region, D region and F region of *h*RXRγ, respectively (Fig. 1A). Notably, the AB region of *h*RXRγ seems to be the most flexible. In addition, *h*RXRγ contains regions (approximately 25% of the analyzed sequence) where the polypeptide chains exhibit context-dependent structural organization (with an S^2 score between 0.69 and 0.8,

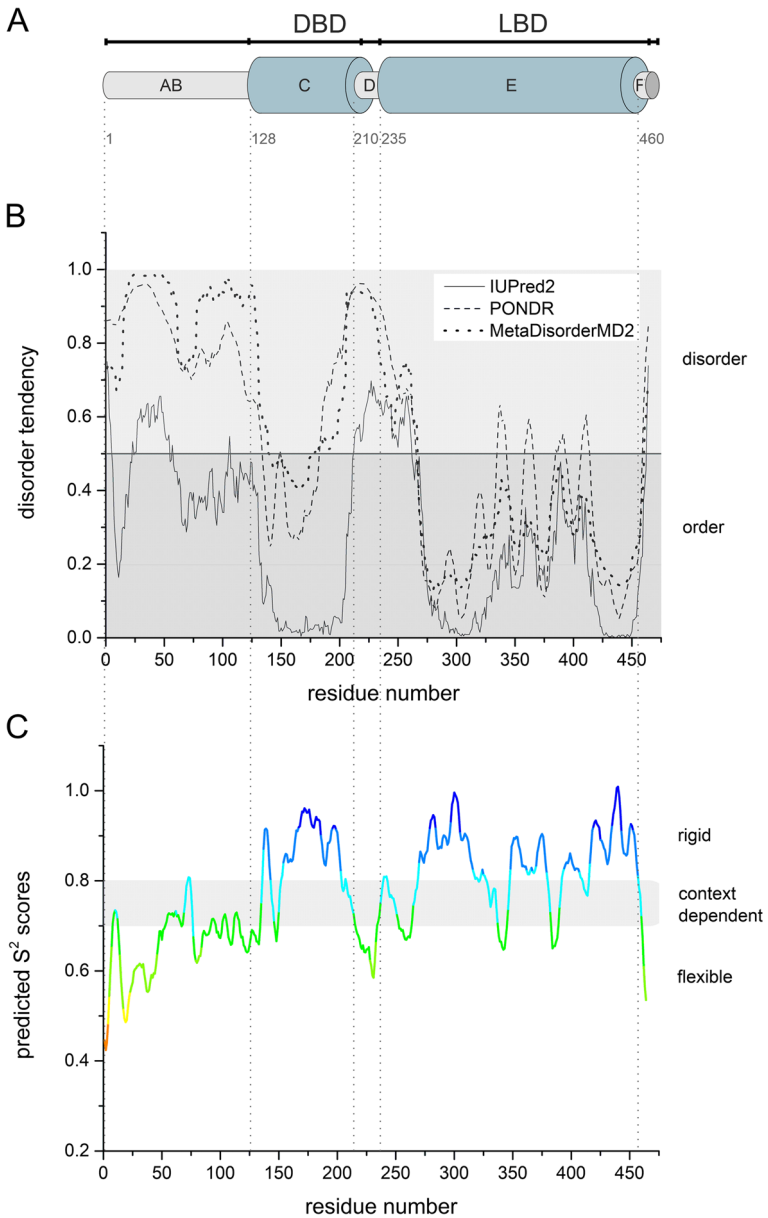

Fig. 1 In silico analysis of the *h*RXRγ sequence. **A** *h*RXRγ exhibits a modular structure with different regions (A–F). Two of the regions correspond to autonomous functional domains: DNA-binding domain (DBD) and ligand-binding domain (LBD). The sequence of the full-length *h*RXRγ was taken from UniProtKB – P48443. Residue numbering corresponds to the boundaries of predicted or experimentally confirmed regions/domains of *h*RXRγ. **B** The prediction of the degree of the disorder in the *h*RXRγ sequence calculated from the primary structure. Three different algorithms were used – IUPred2, PONDR and MetaDisorderMD2. A score above 0.5 indicates a high probability of disorder. **(C)** Prediction of protein backbone dynamics with DynaMine. An S^2 value larger than 0.8 indicates high rigidity of the protein backbone, whereas an S^2 value lower than 0.69 indicates high flexibility, which is typical for disordered segments. Values between 0.69 and 0.8 are characteristic of the context-dependent structural organization of polypeptide chains

which defines the boundary between flexible and rigid protein regions).

To experimentally validate the IDRs in *h*RXRγ, we established an efficient procedure for the expression and purification of *h*RXRγ (Fig. S1) and employed hydrogen–deuterium exchange coupled with mass spectrometry (HDX-MS). This technique allows for the estimation of the exchange rate between deuterons in water and hydrogens in the protein by mass spectrometry. Hydrogen atoms in amide groups that are buried inside the protein or engaged in interactions exhibit much slower exchange rates. Conversely, hydrogen atoms in disordered regions

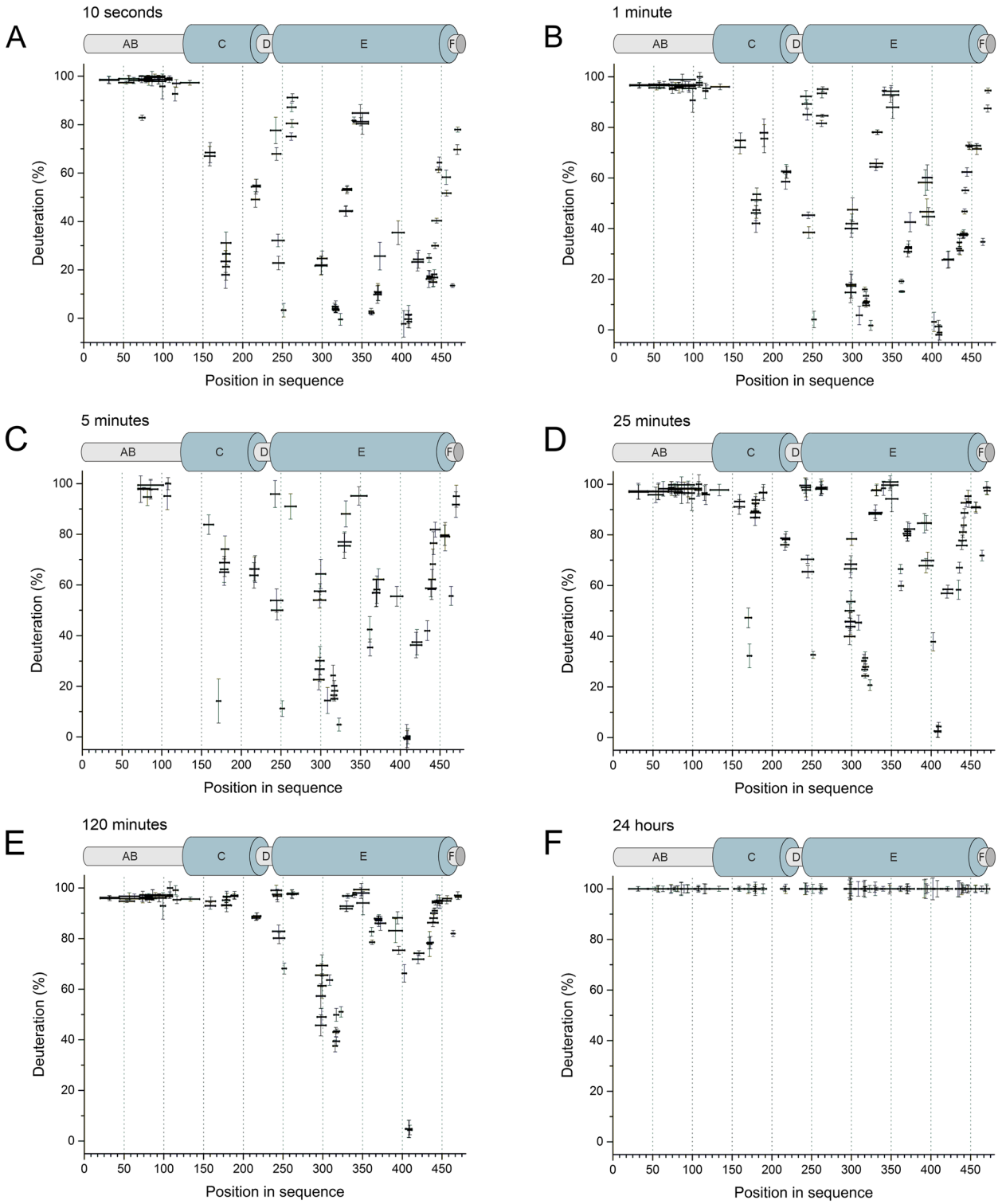

Fig. 2 The hydrogen-deuterium exchange patterns of the *h*RXRγ peptides. The measurements were performed after 10 seconds (**A**), 1 minute (**B**), 5 minutes (**C**), 25 minutes (**D**), 120 minutes (**E**) and 24 hours (**F**) of deuterium exposure at 20 °C. The positioning of peptides in the sequence is shown along the x-axis, represented with a horizontal bar with a length corresponding to a particular peptide. The position of the bar along the y-axis represents the fraction exchanged at the indicated times. Error bars represent standard deviation of four independent measurements

that are not involved in interactions exchange more rapidly. This allows for the experimental identification of IDRs in the protein [54]. The HDX-MS results are presented in Fig. 2, showing the deuteration percentage in distinct regions of *h*RXRγ at various time points. The data indicate that the highest hydrogen exchange rate was observed in the AB region. In fact, almost 100% exchange was observed in the 1–140 amino acid residue region after 10 s of incubation (Fig.2A). This finding is consistent with the results of bioinformatic analyses, which predicted that the AB region is highly disordered (Fig. 1B and C). Other regions identified as disordered by bioinformatic tools, including the 225–260 and 460–464 amino acid residue regions, also exhibited significant exchange after 10 s of incubation, with this effect increasing further with longer incubation times. The HDX-MS data also revealed that DBD (128–210 amino acid residues) in full-length *h*RXRγ exhibited faster hydrogen exchange compared to LBD (235–460 amino acid residues), suggesting a higher degree of disorder in DBD (Fig. 2E). This contrasts with in silico predictions, which indicated a stronger propensity for an ordered structure in DBD compared to LBD (Fig. 1B). Interestingly, although in silico analysis predicted a higher disorder tendency for LBD (Fig. 1B), HDX-MS showed slower hydrogen exchange in this region (Fig. 2E). Notably, two regions within LBD, spanning amino acid residues 275–325 and 420–450, remained unexchanged even after 120 min. This aligns with in silico predictions, which classified these regions as ordered/rigid (Fig. 1B). After overnight incubation, 100% exchange was observed for the entire protein (Fig. 2F).

Together, the results of the in silico analysis and HDX-MS indicate that the AB region of *h*RXRγ in the context of the full-length protein is intrinsically disordered.

Analysis of the oligomerization states of *h*RXRγ and ΔAB*h*RXRγ

RXR integrates and modulates diverse cellular processes through its ability to form heterodimers with other NRs [17]. Moreover, RXR can assemble into homodimers and homotetramers [18, 25–27]. Despite its importance, the molecular mechanisms underlying RXR's oligomerization and interactions remain largely unexplored. During purification, both *h*RXRγ and ΔAB*h*RXRγ displayed a tendency to oligomerization, as indicated by their elution in multiple peaks (**Fig. S1** and **S2**). To further investigate this tendency, chemical cross-linking experiments followed by SDS-PAGE were performed (data not shown). A water-soluble BS^3 crosslinker, which reacts with primary amino groups on the target protein via NHS esters to form stable amide bonds, was selected for this analysis. Cross-linking of *h*RXRγ with BS^3 resulted in distinct bands corresponding to monomers, dimers, and higher-order oligomers. In contrast, cross-linking of ΔAB*h*RXRγ revealed mainly monomers and dimers. These results indicate that both *h*RXRγ and ΔAB*h*RXRγ can form oligomers; however, ΔAB*h*RXRγ assembles into smaller oligomeric forms compared to the higher-order oligomers observed for *h*RXRγ. These findings suggest that the AB region in the full-length *h*RXRγ modulates the formation of higher-order oligomeric forms.

To further analyze the influence of the intrinsically disordered AB region on the oligomerization of *h*RXRγ, size-exclusion chromatography coupled with multi-angle light scattering (SEC-MALS) was performed. This combination of SEC for separation and MALS for analysis allows for conformation- and shape-independent determination of the molecular weights of analyzed macromolecules [55]. However, we encountered challenges in obtaining conclusive results for the *h*RXRγ and ΔAB*h*RXRγ samples prepared using the routine purification procedure (see Methods, Fig. S1, and Fig. S2) as the complexity of the size distribution exceeded the resolution capacity of SEC (data not shown). Therefore, for SEC-MALS analysis, we employed prefractionated populations of both proteins. During the SEC purification step, *h*RXRγ and ΔAB*h*RXRγ fractions were separated into two categories: *h*RXRγ_oligomer and ΔAB*h*RXRγ_oligomer (first peak, smaller elution volume) and *h*RXRγ_dimer and ΔAB*h*RXRγ _dimer (second peak, larger elution volume) (Fig. S1 and Fig. S2). Each prefractionated sample was analyzed separately by SEC-MALS at a concentration of 5 mg/ml (Fig. 3). In the *h*RXRγ_oligomer sample, there was almost exclusively a higher-order oligomer, with a small fraction of homodimers (Fig. 3A). In contrast, the *h*RXRγ_dimer sample contained a mixture of monomers, homodimers, and higher-order oligomers (Fig. 3B). For both samples, the exact size of oligomeric fraction of *h*RXRγ could not be definitively determined. It might be a homotetramer, homopentamer, homohexamer, or a mixture of these. The SEC-MALS data were more conclusive for ΔAB*h*RXRγ. The analysis for the ΔAB*h*RXRγ_oligomer sample (Fig. 3C) indicated the presence of monomers and homotetramers, while the ΔAB*h*RXRγ_dimer sample (Fig. 3D) contained monomers and homodimers

Summarizing, SEC-MALS data demonstrated that *h*RXRγ in solution exists as a monomer, dimer and higher-order oligomers (likely homotetramer, homopentamer, or homohexamer), whereas ΔAB*h*RXRγ primarily exists as a monomer, homodimer and homotetramer. These findings confirmed the chemical cross-linking results, indicating that the inherently disordered AB region controls the oligomerization tendency of *h*RXRγ. While both *h*RXRγ and ΔAB*h*RXRγ can form oligomers, *h*RXRγ assembles into higher-order oligomers compared to the smaller oligomeric forms observed for ΔAB*h*RXRγ.

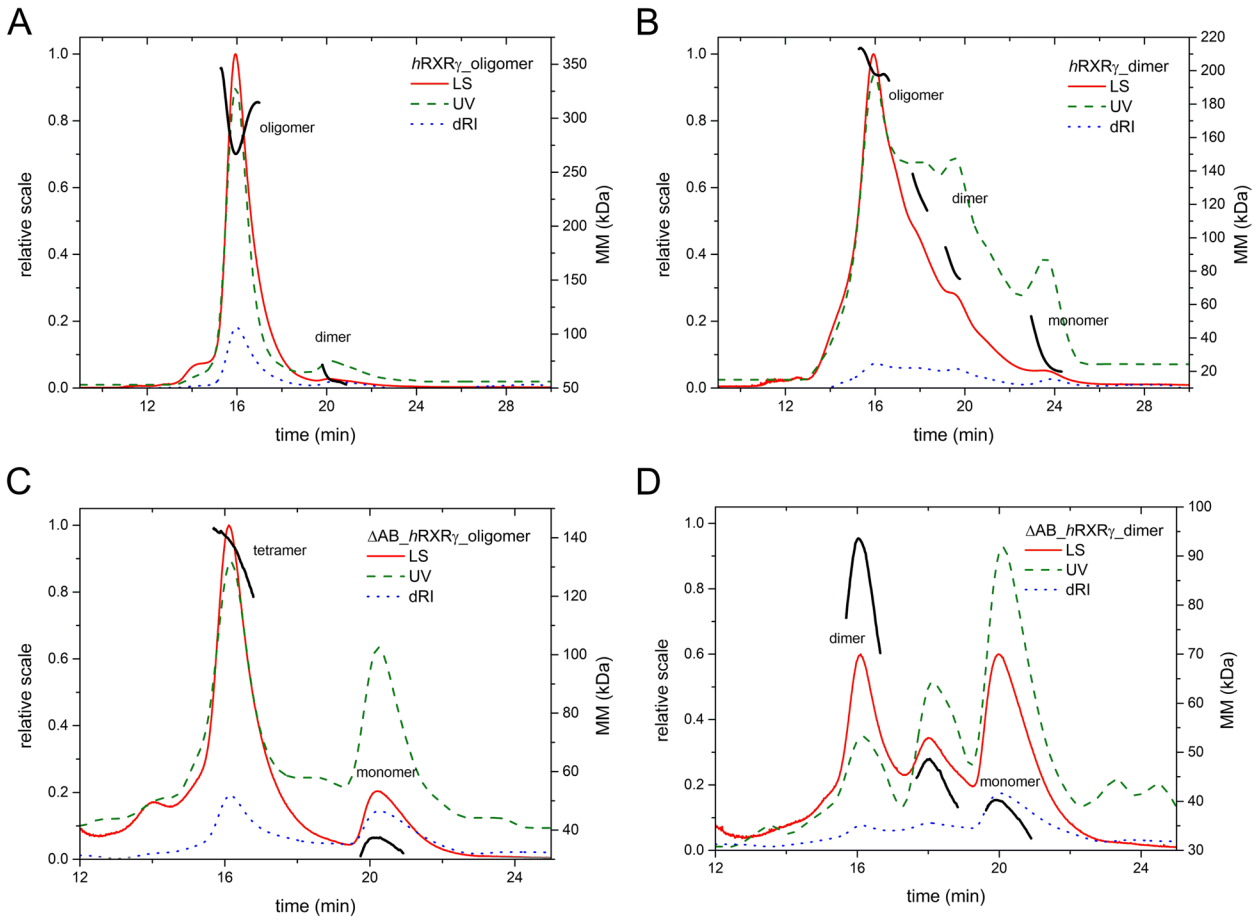

Fig. 3 Analysis of the oligomeric states of *h*RXRγ and DAB *h*RXRγ by SEC-MALS. SEC-MALS experiments were performed for (**A**) *h*RXRγ_oligomer, (**B**) *h*RXRγ_dimer, (**C**) DAB*h*RXRγ_oligomer and (**D**) DAB*h*RXRγ_dimer samples. In each chromatogram, the red solid line represents light scattering (LC), the green dashed line represents absorbance measured at 280 nm (UV), the blue dotted line represents refractive index (dRI), and the black lines represents average MM values (right axis)

Additionally, SEC-MALS analysis revealed that the AB region acts as structural element stabilizing *h*RXRγ's higher-order oligomeric states, as *h*RXRγ shows a greater tendency to form stable oligomers in solution. The intrinsically disordered AB region is thus a critical determinant of the molecular properties of *h*RXRγ, and its deletion significantly impacts the receptor molecule's tendency to oligomerize.

Study of the hydrodynamic properties of *h*RXRγ and ΔAB*h*RXRγ by analytical ultracentrifugation

To further evaluate the effect of the AB region on the oligomerization propensity of RXR, the hydrodynamic properties of the prefractionated populations—*h*RXRγ_oligomer, ΔAB*h*RXRγ_oligomer, *h*RXRγ_dimer and ΔAB*h*RXRγ_dimer—were analyzed using sedimentation velocity analytical ultracentrifugation (SV-AUC). This biophysical method enables the study of proteins and their interactions in solution based on their mass- and shape-dependent migration in a centrifugal field [56]. Each sample (*h*RXRγ_oligomer, *h*RXRγ_dimer, ΔAB*h*RXRγ_oligomer, and ΔAB*h*RXRγ_dimer) was analyzed at three different concentrations: 0.8 mg/ml, 0.4 mg/ml and 0.2 mg/ml. Data analysis for all three concentrations yielded a good fit (RMSD; Table 1, Fig. S3). No significant dependence of the sedimentation coefficient ($s_{20,w}$) on the protein concentration was observed (Table 1). The collected frictional ratio (f/f_0) data enabled to define the character of the analyzed proteins. Globular proteins are characterized by values of approximately 1.2–1.25, which do not change a lot with an increase of molecular mass (f/f_0 ratios are 1.19–1.25 for the 20 − 200 kDa globular proteins) [57, 58]. The calculated f/f_0 ratio for four analyzed samples is 1.2 (Table 1), which classified *h*RXRγ and ΔAB*h*RXRγ as globular proteins.

Sedimentation coefficient distributions calculated from the SV-AUC data indicated that the *h*RXRγ_oligomer species have sedimentation coefficients ($s_{20,w}$)

Table 1 Hydrodynamic properties of *h*RXRγ and ΔAB*h*RXRγ obtained by SV-AUC analysis

Protein	c [mg/ml]	RMSD	f/f_0	MW [kDa]	R_s [Å]	$s_{(20,w)}$ [S]
*h*RXRγ "oligomer"	0.2	0.007920	1.219780	88.0 259	36.0 51.5	5.753 11.827
	0.4	0.007786	1.229020	87.3 257	36.1 51.8	5.679 11.678
	0.8	0.008308	1.219780	88.0 259	36.0 51.5	5.753 11.827
*h*RXRγ "dimer"	0.2	0.008700	1.212412	97.9 249	37.0 50.6	6.215 11.590
	0.4	0.008976	1.232288	101 242	38.0 50.9	6.249 11.192
	0.8	0.010549	1.238849	106 237	39.8 50.8	6.421 10.977
ΔAB*h*RXRγ "oligomer"	0.2	0.008059	1.209588	80.7 238	34.7 49.7	5.435 11.181
	0.4	0.008496	1.192068	87.4 236	35.1 48.8	5.817 11.276
	0.8	0.009450	1.201445	93.0 230	36.1 48.8	6.015 11.000
ΔAB*h*RXRγ "dimer"	0.2	0.008813	1.210089	95.1 228	36.6 49.0	6.067 10.865
	0.4	0.009382	1.196605	114	38.4	6.904
	0.8	0.010962	1.210319	122	39.9	7.173

of approximately 5.7 S and 11.8 S, respectively (Fig. 4A, Table 1). The estimated molecular masses (88 kDa and 259 Da) were close to the theoretical values of homodimer (101 kDa) and homopentamer (254 kDa). Similar results were obtained for the *h*RXRγ_dimer sample (the sedimentation coefficients ($s_{20,w}$) of approximately 6.3 S and 11.2 S were observed) (Fig. 4B, Table 1). The estimated molecular masses (102 kDa and 243 Da) were also close to the theoretical values of homodimer and homopentamer. Although both analyzed *h*RXRγ samples appeared to contain the same two main species, their proportions differed. The dominant species in the *h*RXRγ_oligomer sample was homopentamer, whereas in the *h*RXRγ_dimer sample, it was homodimer. Under the same conditions, the SV-AUC analysis of the ΔAB*h*RXRγ_oligomer sample, identified two species with the sedimentation coefficients ($s_{20,w}$) of approximately 5.7 S and 11.1 S, respectively (Fig. 4C, Table 1). The estimated molecular masses (87 kDa and 235 Da) were close to the theoretical values of homodimer (76.6 kDa) and homohexamer (230 kDa). The major population of molecules in the ΔAB*h*RXRγ_oligomer sample existed as homohexamer. The sedimentation coefficient distributions calculated from the SV-AUC data indicated two species in the ΔAB*h*RXRγ_dimer sample, with sedimentation coefficients ($s_{20,w}$) of approximately 6.7 S and 10.9 S, respectively (Fig. 4D, Table 1). Although the estimated molecular masses (110 kDa and 228 kDa) were close to the theoretical values of homotrimer (115 kDa) and homohexamer (230 kDa), the low resolution and overlapping peaks suggest that the main species could also be homodimer, with a tendency to form higher-order oligomers.

In conclusion, the *h*RXRγ_oligomer and ΔAB*h*RXRγ_oligomer samples predominantly contained higher-order oligomeric forms, which appeared to be stable once formed. In contrast, the *h*RXRγ_dimer and ΔAB*h*RXRγ_dimer samples exhibited a dynamic equilibrium, particularly noticeable in the ΔAB*h*RXRγ_dimer sample. This finding highlights distinct oligomerization tendencies in *h*RXRγ and ΔAB*h*RXRγ, which are dependent on the presence of the AB region.

Impact of ionic strength on the secondary and tertiary structures of *h*RXRγ and ΔAB*h*RXRγ

To evaluate the effect of the AB region on the molecular properties of *h*RXRγ, both the full-length protein (*h*RXRγ) and the deletion mutant (ΔAB*h*RXRγ), prepared using the routine procedure (see Methods), were examined under varying ionic strength conditions using circular dichroism (CD) spectroscopy [59, 60]. The secondary structures of *h*RXRγ and ΔAB*h*RXRγ were analyzed at two NaCl concentrations: 50 mM and 300 mM. In all cases, the CD spectra (Fig. 5) displayed characteristic deep negative maxima at approximately 208 and 222 nm, indicative of ordered secondary structures [61].

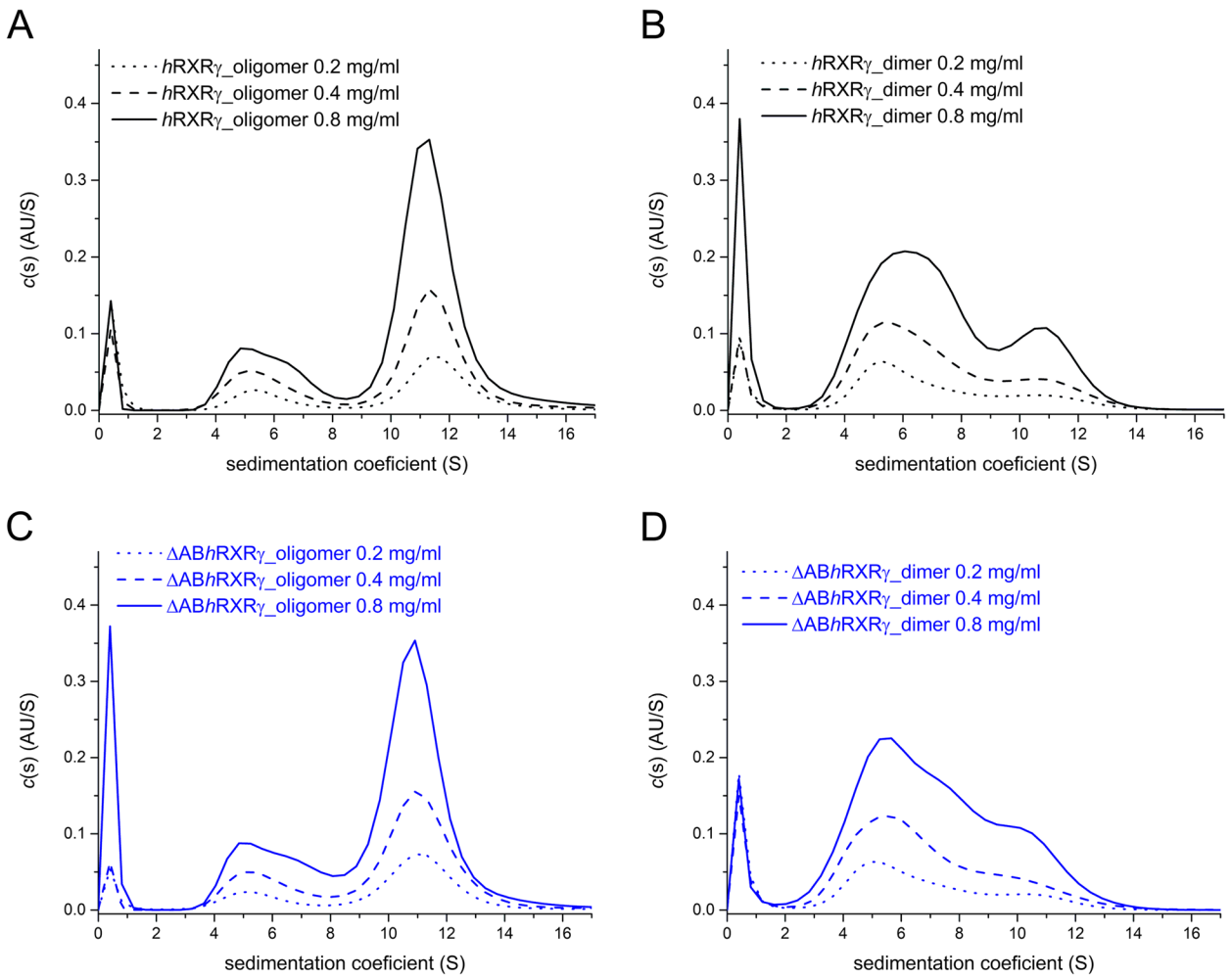

Fig. 4 Sedimentation velocity analysis (SC-AUC).Superposition of the sedimentation coefficient *c*(s) distributions of *h*RXRγ_oligomer (**A**), *h*RXRγ_dimer (**B**), DAB*h*RXRγ_oligomer (**C**) and DAB*h*RXRγ_dimer (**D**) for three different concentrations: 0.2 mg/ml (dotted line), 0.4 mg/ml (dashed line) and 0.8 mg/ml (solid line)

Although both *h*RXRγ and ΔAB*h*RXRγ exhibited a high percentage of ordered structures at 50 mM and 300 mM NaCl, differences in their spectra were observed. To estimate the content of secondary structures in *h*RXRγ and ΔAB*h*RXRγ at both NaCl concentrations, the CDPro software package was used with the Continll, Selon3 and Cdsstr algorithms [44]. The obtained and averaged results are summarized in Table 2. While the CD data were collected down to 205 nm due to buffer absorbance limitations, this spectral range was sufficient to observe clear and reproducible trends in secondary structure content across conditions and constructs. At 50 mM NaCl, the predominant ordered structure in *h*RXRγ was α-helix (38 ± 2.1%). The β-strand content was estimated at 16 ± 1.8%. The analysis also indicated the presence of a significant number of unordered regions (31 ± 2.0%). The content of the turns was determined to be 15 ± 1.2%. Increasing the NaCl concentration to 300 mM altered the secondary structure composition of *h*RXRγ, resulting in a decrease in α-helix content to 30 ± 2.8%, accompanied by increases in β-strand (18 ± 2.9%), turns (19 ± 2.0%), and unordered regions (33 ± 1.4%).

The analysis of ΔAB*h*RXRγ at 50 mM NaCl revealed an α-helix content of 20 ± 2.1% and a β-strand content of 27 ± 4.8% (Table 2). Additionally, the content of turns and unordered regions was estimated at 20 ± 0.7% and 33 ± 6.3%, respectively. Higher (300 mM) NaCl concentration led to a significant increase in α-helix (36 ± 3.0%) content of ΔAB*h*RXRγ. A simultaneous decrease in the β-strand (20 ± 4.1%), turns (16 ± 1.1) and unordered (28 ± 4.8%) content of ΔAB*h*RXRγ (50 mM NaCl) was observed. These changes were the opposite to those observed for *h*RXRγ, where an increase in ionic strength

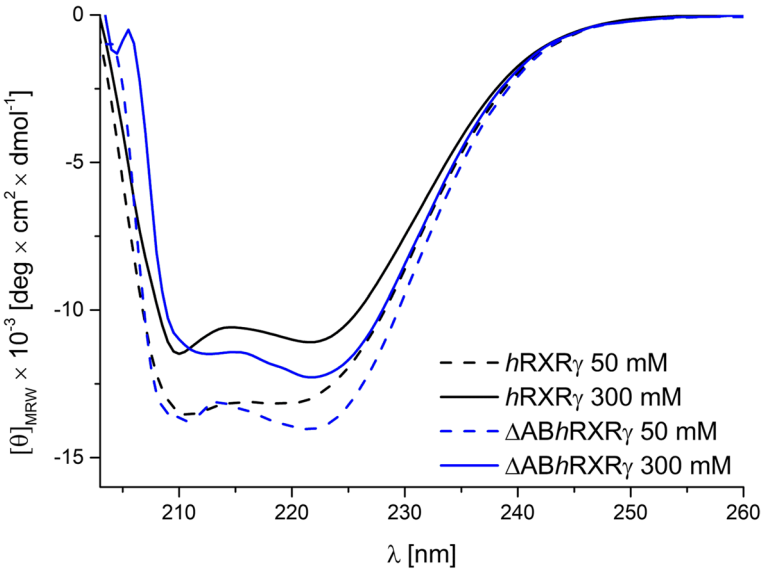

Fig. 5 Ionic strength-induced changes in the secondary structure of *h*RXRγ and DAB*h*RXRγ.Far-UV spectra of *h*RXRγ and DAB*h*RXRγ recorded at different NaCl concentrations (50 mM NaCl – dashed lines; 300 mM NaCl – solid lines). Protein concentrations were 10 µM, and spectra were measured at 20 °C

Table 2 Estimation of secondary structure content in *h*RXRγ and ΔAB*h*RXRγ derived from CD spectra

protein	α-helix [%]			β-strand [%]			turns [%]	unordered [%]
	regular	distorted	total	regular	distorted	total		
*h*RXRγ_50	21 ± 1.4	17 ± 0.7	38 ± 2.1	8 ± 0.9	8 ± 0.9	16 ± 1.8	15 ± 1.2	31 ± 2.0
*h*RXRγ_300	17 ± 2.2	13 ± 0.6	30 ± 2.8	11 ± 1.0	7 ± 1.9	18 ± 2.9	19 ± 2.0	33 ± 1.4
ΔAB*h*RXRγ_50	12 ± 0.4	8 ± 1.7	20 ± 2.1	12 ± 2.9	15 ± 1.9	27 ± 4.8	20 ± 0.7	33 ± 6.3
ΔAB*h*RXRγ_300	20 ± 2.1	16 ± 0.9	36 ± 3.0	12 ± 2.3	8 ± 1.9	20 ± 4.1	16 ± 1.1	28 ± 4.8
mixture (AB region and ΔAB*h*RXRγ)	23 ± 2.7	21 ± 0.5	44 ± 3.2	8 ± 1.3	16 ± 0.9	23 ± 2.2	15 ± 1.3	18 ± 2.0
sum (AB region and ΔAB*h*RXRγ)	21 ± 0.9	27 ± 1.2	48 ± 2.1	6 ± 1.7	6 ± 1.3	12 ± 3.0	12 ± 2.8	28 ± 3.7

led to a decrease in α-helix content, accompanied by an increase in β-strand, turns, and unordered structures.

These results highlight a distinct difference in how *h*RXRγ and ΔAB*h*RXRγ respond to changes in ionic strength. Our data suggest that the AB region contributes to the conformational behavior and ionic sensitivity of the structured domains (DBD and LBD) in *h*RXRγ. This effect is reflected in a reduction in α-helix content, most likely within these domains. In contrast, the increase in α-helix content observed in ΔAB*h*RXRγ at 300 mM NaCl suggests that the absence of the AB region allows for enhanced structural ordering under these conditions. These findings underscore the role of the AB region as a critical modulator of the conformational states of *h*RXRγ and its responsiveness to environmental factors, such as ionic strength.

Far-UV spectra of *h*RXRγ and ΔAB*h*RXRγ recorded at different NaCl concentrations (50 mM NaCl – dashed lines; 300 mM NaCl – solid lines). Protein concentrations were 10 µM, and spectra were measured at 20 °C.

To further evaluate the impact of the AB region on the molecular properties of RXR, the effect of temperature on the secondary structures of *h*RXRγ and ΔAB*h*RXRγ at 50 mM and 300 mM NaCl was analyzed using far-UV CD spectroscopy (Fig. 6 and Fig. S4). Heating of the *h*RXRγ sample from 25 to 65 °C in the presence of 50 mM (Fig. S4 A) and 300 mM NaCl (Fig. S4B) resulted in a thermally induced conformational transition, characteristic of the typical unfolding process observed in ordered globular proteins. Thermal denaturation was also monitored by CD spectroscopy at 222 nm, a wavelength characteristic of α-helical content (Fig. 6A). The main temperature transitions for *h*RXRγ were observed at 41 °C and 42 °C for 50 mM and 300 mM NaCl, respectively. Notably, the denaturation process for *h*RXRγ exhibited a multiphasic profile, particularly evident at low ionic strength (50

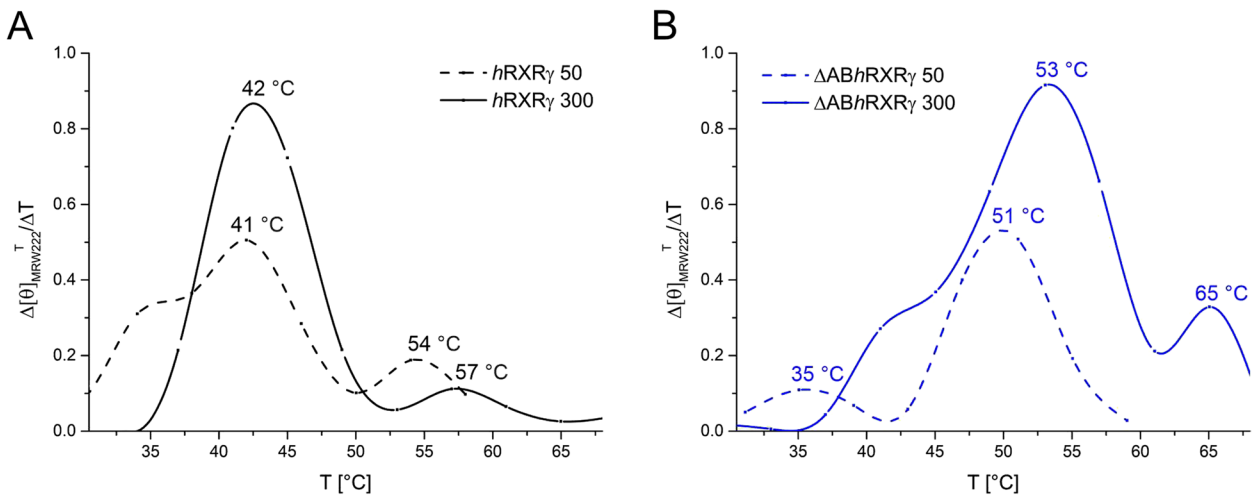

Fig. 6 The effect of temperature on *h*RXRγ and DAB*h*RXRγ. First-order derivative plot of the melting curves for *h*RXRγ (**A**) and DAB*h*RXRγ (**B**). The plots display the first-order derivatives of ellipticity at 222 nm with respect to temperature, measured over a range of 30 to 70 °C ($d[q]_{MRW222}/dT$). Protein concentrations were 10 μM. The curves represent *h*RXRγ at 50 mM NaCl (black dashed line) and 300 mM NaCl (black solid line), and DAB*h*RXRγ at 50 mM NaCl (blue dashed line) and 300 mM NaCl (blue solid line)

mM NaCl), in the first-order derivative plot of the melting curves (Fig. 6A), reflecting the multidomain nature of RXR. These results indicate that increased ionic strength provides enhanced stability to the secondary structure of *h*RXRγ, as demonstrated by the slightly higher transition temperature at 300 mM NaCl.

The effect of temperature on the conformation of ΔAB*h*RXRγ was also investigated by CD analysis over a temperature range of 25 to 65 °C (Fig. S4 C and S4D). Structural changes induced by increasing temperature were observed at both 50 mM (Fig. S4 C) and 300 mM NaCl (Fig. S4D). Like *h*RXRγ, ΔAB*h*RXRγ exhibited increased stability at higher ionic strength. However, the main transition temperatures for ΔAB*h*RXRγ were 51 °C and 53 °C at 50 mM and 300 mM NaCl, respectively (Fig. 6B). The results indicate that ΔAB*h*RXRγ, lacking the AB region, was more resistant to higher temperatures than *h*RXRγ, as its transition temperature was at least 10 °C higher. The denaturation process for ΔAB*h*RXRγ also exhibited a multiphasic profile, similarly as it was observed to *h*RXRγ.

Thus, the AB region appears to act as a critical factor modulating the stability and conformational states of *h*RXRγ. The presence of the AB region reduces the thermal stability of *h*RXRγ, likely due to its association with the rest of the protein. This suggests that the AB region does not function as an independent entity but rather integrates into the overall *h*RXRγ structure, influencing its folding and stability.

First-order derivative plot of the melting curves for *h*RXRγ **(A)** and ΔAB*h*RXRγ **(B)**. The plots display the first-order derivatives of ellipticity at 222 nm with respect to temperature, measured over a range of 30 to 70 °C ($d[\theta]_{MRW222}/dT$). Protein concentrations were 10 μM. The curves represent *h*RXRγ at 50 mM NaCl (black dashed line) and 300 mM NaCl (black solid line), and ΔAB*h*RXRγ at 50 mM NaCl (blue dashed line) and 300 mM NaCl (blue solid line).

After establishing the secondary structures of *h*RXRγ and ΔAB*h*RXRγ at 50 mM and 300 mM NaCl, ANS fluorescence spectroscopy experiments were employed to further investigate the molecular properties of both proteins (Fig. 7). By measuring the fluorescence intensity and emission maxima of ANS under different ionic strength conditions, additional insights into the hydrophobicity and potential structural changes of *h*RXRγ and ΔAB*h*RXRγ, which might not be captured by CD alone were obtained. Free ANS exhibits a fluorescence spectrum characterized by a low emission maximum at 525 nm. Upon binding to the hydrophobic surfaces of proteins, the fluorescence of ANS significantly increases [62]. As shown in Fig. 7, upon the addition of proteins, the fluorescence intensity of ANS increased 5.8-fold for *h*RXRγ and 21.8-fold for ΔAB*h*RXRγ at 50 mM NaCl. The position of the fluorescence maxima blueshifted from 526 to 463 nm and 457 nm, respectively, due to association of the probe to the proteins. These findings suggest that ΔAB*h*RXRγ has distinct molecular properties, with more hydrophobic surfaces exposed than *h*RXRγ, which is likely linked to the AB region. Moreover, a slight decrease in fluorescence intensity was observed upon increasing the NaCl concentration to 300 mM (Fig. 7), with

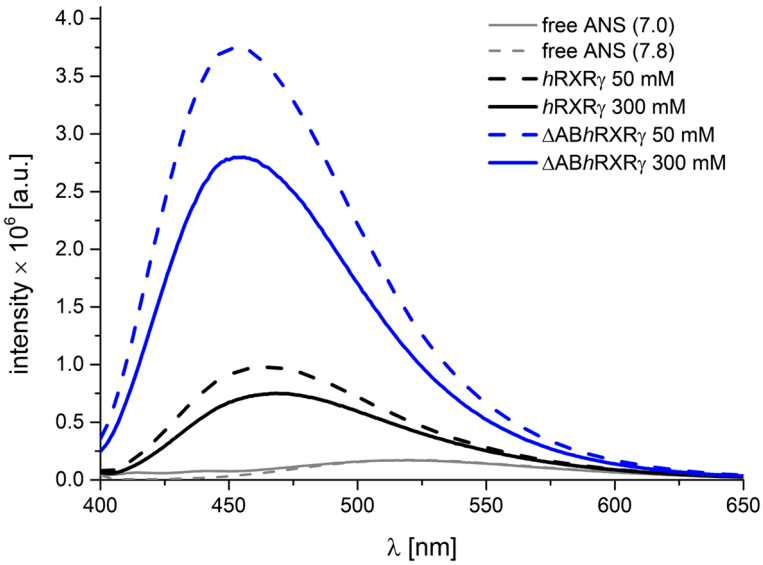

Fig. 7 Fluorescence spectra of *h*RXRγ and DAB*h*RXRγ. Fluorescence spectra of ANS binding to *h*RXRγ and DAB*h*RXRγ at 50 mM (dashed black and blue lines, respectively) and 300 mM (solid black and blue lines, respectively) NaCl concentrations. The spectra of free ANS (solid and dashed grey lines) are also shown. Protein samples (*h*RXRγ and ΔAB*h*RXRγ) were prepared at a concentration of 2 μM with 20 μM ANS

fluorescence intensity values of 4.5-fold for *h*RXRγ and 16.4-fold for ΔAB*h*RXRγ. Concomitantly, an additional blue shift of 5 nm and 1 nm in the emission maxima was observed, for *h*RXRγ and ΔAB*h*RXRγ, respectively. This suggests more extensive structural rearrangement in the hydrophobic regions of *h*RXRγ.

These data complement the secondary structure analysis and allow for the evaluation of the impact of the AB region on molecular properties of *h*RXRγ. The increased exposure of hydrophobic residues, as revealed by ANS fluorescence experiments, contributed to the enhanced thermal stability of ΔAB*h*RXRγ. Hydrophobic interactions are known to play a significant role in maintaining protein structure, and their increased presence could help stabilize the protein's conformation at elevated temperatures [63, 64]. In contrast, the presence of the AB region in *h*RXRγ alters hydrophobicity, leading to decreased stability at elevated temperatures. This effect can be attributed to both the integration and interaction of the AB region with the rest of the protein, which likely alters parts of the hydrophobic surfaces and weakens their stabilizing interactions.

Fluorescence spectra of ANS binding to *h*RXRγ and ΔAB*h*RXRγ at 50 mM (dashed black and blue lines, respectively) and 300 mM (solid black and blue lines, respectively) NaCl concentrations. The spectra of free ANS (solid and dashed grey lines) are also shown. Protein samples (*h*RXRγ and ΔAB*h*RXRγ) were prepared at a concentration of 2 μM with 20 μM ANS.

Impact of ionic strength, hormone response element and ligand on the structure of RXR investigated with limited proteolysis

Limited proteolysis experiments were used to delineate the further structural differences between the *h*RXRγ and ΔAB*h*RXRγ, as well as to highlight the role of the AB region as a critical modulator of the receptor's structure (Fig. 8). The digestion of both *h*RXRγ and ΔAB*h*RXRγ was performed at 50 mM (Fig. 8A and E) and 300 mM (Fig. 8B and F) NaCl and additionally in the presence of the RXR hormone response element, *Ramp2* DR1 DNA (Fig. 8C and G) and RXR ligand, 9-*cis*-retinoic acid (Fig. 8D and H). The glutamyl endopeptidase Glu-C (V8) from *Staphylococcus aureus* [65], which preferentially cleaves at the C-terminus of either Glu or Asp residues, was utilized. The *h*RXRγ sequence analysis using a PeptideCutter [46] indicated that there are 29 putative cleavage sites for V8 (AB region: 1; DBD: 2; D region: 7; LBD: 19). V8 is stable and its activity does not change in the presence of tested conditions. *h*RXRγ and ΔAB*h*RXRγ, either alone or under specific conditions, remained stable during a 4-h incubation period (Fig. 8A-H, lane 10). *h*RXRγ in the presence of 50 mM NaCl (*h*RXRγ 50 mM) was the most sensitive to protease V8 digestion (Fig. 8A). The band corresponding to the intact protein completely disappeared after 2 h of incubation (Fig. 8A, lane 8). In contrast, the cleavage sites of *h*RXRγ in the presence of 300 mM NaCl (*h*RXRγ 300 mM) were less accessible to protease (Fig. 8B). After 2 h, the band corresponding to the intact protein was still detectable (Fig. 8B, lane 8).

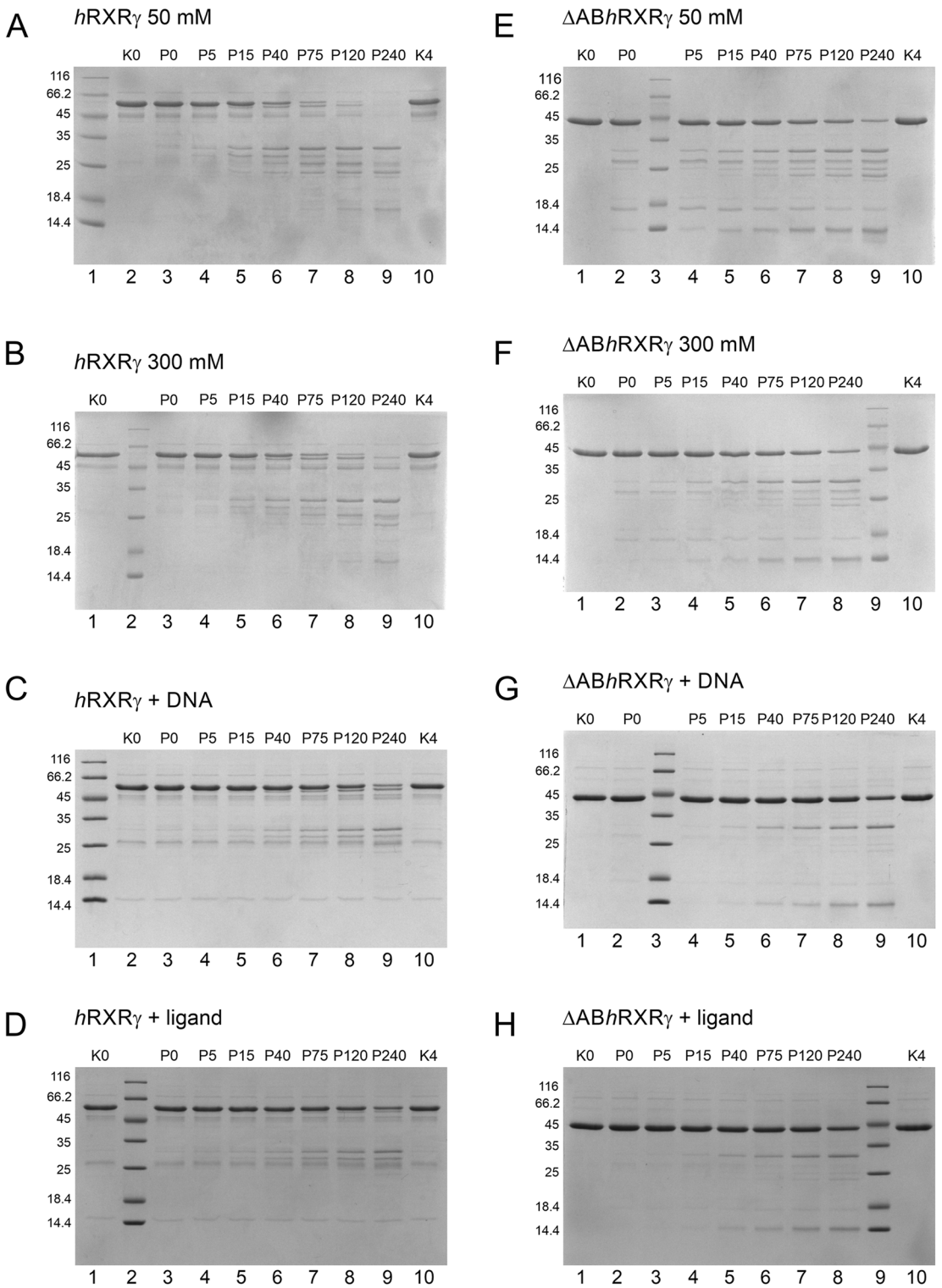

Fig. 8 Effect of ionic strength, DNA and ligand on the proteolysis of *h*RXRγ and DAB*h*RXRγ by V8 protease. SDS-PAGE analysis of limited proteolysis products at different NaCl concentrations (**A**-**B**) and (**E**-**F**), in the presence of DNA (**C**) and (**G**) and in the presence of ligand (**D**) and (**H**). Both *h*RXRγ and DAB*h*RXRγ were incubated with V8 protease at 25 °C at an enzyme-to-substrate ratio of 1:250 (w/w). The control reactions (K0 and K4) did not contain enzyme. The molecular weight marker is shown on the left of each gel in kDa. The aliquots were taken at 5 min, 15 min, 40 min, 75 min, 120 min and after 240 min after the addition of enzyme

These results indicate that under higher ionic strength, the *h*RXRγ protein was more resistant to digestion.

Under the same conditions, digestion of ΔAB*h*RXRγ resulted in the presence of a significant amount of the intact protein in the reaction mixture (Fig. 8E and F). The band corresponding to the intact protein remained, to some extent, unaffected even after 240 min of incubation (Fig. 8E**, lane 9 and** Fig. 8F**, lane 8**). This result is particularly interesting, as the AB region contains only a single cleavage site for V8 protease, yet its presence in *h*RXRγ appears to enhance the accessibility of cleavage sites outside this region. These observations align with ANS fluorescence data, which revealed that the AB region reduces the accessibility of hydrophobic residues, potentially by interacting with the structured domains such as DBD or LBD, thereby influencing V8 protease susceptibility. By interacting with the rest of the protein, the AB region appears to destabilize it, possibly introducing numerous transient interactions that induce a range of conformational states, including those that expose otherwise protected residues to V8 protease.

The digestion in the presence of DNA (*h*RXRγ + DNA) and ligand (*h*RXRγ + ligand) appeared to be greatly retarded, with the *h*RXRγ protein still present in the reaction mixture after 4 h (Fig. 8C and D, lane 9). Interestingly, the digestion patterns of *h*RXRγ in the presence of DNA (Fig. 8C) and ligand (Fig. 8D) appeared to be similar but different compared to the patterns obtained for the unbound protein (Fig. 8A and B). Upon DNA/ligand binding, RXR underwent structural rearrangements and turned out to be more resistant to the V8 digestion. Additionally, *h*RXRγ protein turned out to be more resistant to the digestion in the presence of ligand in comparison to the presence of DNA (Fig. 8C and Fig. 8D, lane 9) as the band corresponding to intact protein was more intense. Still *h*RXRγ in the presence of DNA and ligand was more susceptible to proteolysis in comparison to ΔAB*h*RXRγ under the same conditions (Fig. 8G, lane 9 and Fig. 8H, lane 8). The band corresponding to the intact protein is more intense. Additionally, in the presence of DNA and ligand, distinct band patterns were observed for *h*RXRγ and ΔAB*h*RXRγ, likely reflecting variations in their conformational states.

Limited proteolysis enabled the detection of structural rearrangements induced by ionic strength, DNA, and ligand binding. The results provide further evidence that the AB region modulates conformation of the structured domains, including DBD and LBD. DNA or ligand binding stabilizes the structured core of the protein, which, in turn, influences the communication and interaction between the structured core and the intrinsically disordered AB region, redefining their conformational states.

SDS-PAGE analysis of limited proteolysis products at different NaCl concentrations (**A-B**) and (**E–F**), in the presence of DNA (**C**) and (**G**) and in the presence of ligand (**D**) and (**H**). Both *h*RXRγ and ΔAB*h*RXRγ were incubated with V8 protease at 25 °C at an enzyme-to-substrate ratio of 1:250 (w/w). The control reactions (K0 and K4) did not contain enzyme. The molecular weight marker is shown on the left of each gel in kDa. The aliquots were taken at 5 min, 15 min, 40 min, 75 min, 120 min and after 240 min after the addition of enzyme.

Binding of the AB region to ΔAB*h*RXRγ induces conformational changes

The results presented above demonstrated that the AB region modulates the molecular properties of *h*RXRγ. We decided to examine whether this is solely a consequence of the presence of this fragment within the *h*RXRγ polypeptide or if it also results from its interaction with another part of the protein. IDRs are known to regulate the activity of TFs through intramolecular interactions with structured domains [11, 12]. For steroid nuclear receptors, physical intramolecular associations between the N-terminal (AB region) and C-terminal domains (LBD) have been reported [66–68].

To explore whether such interaction may occur in *h*RXRγ, we analyzed the AlphaFold-predicted structure of the full-length receptor (**Figure S5**). The model suggests a potential for transient intramolecular contacts between the AB region and the rest of the protein. Although AlphaFold has limitations in modeling the dynamic behavior of IDRs, the prediction indicates a possible spatial proximity between the AB region and LBD—reminiscent of intramolecular interactions reported for steroid receptors. To further investigate the potential interaction between the intrinsically disordered AB region and the globular ΔAB*h*RXRγ, CD experiments were performed. The CD spectra of ΔAB*h*RXRγ, the AB region of *h*RXRγ, and a mixture of the two were recorded (Fig. 9). The AB region spectrum displayed a pronounced minimum at 205 nm (Fig. 9), characteristic of disordered regions, and was consistent with previously published spectra of the AB region [33]. To evaluate the interaction between the AB region and ΔAB*h*RXRγ, an additive spectrum was calculated by summing the individual spectra of the two proteins. This calculated spectrum was then compared with the spectrum of the mixed sample. Notable differences between the mixed sample and the additive spectrum (Fig. 9) suggest that the interaction between the AB region and ΔAB*h*RXRγ induces conformational changes in one or both proteins.

The secondary structure content of the mixed sample and the calculated additive spectrum was analyzed using the CDPro software package (Table 2). The mixed sample

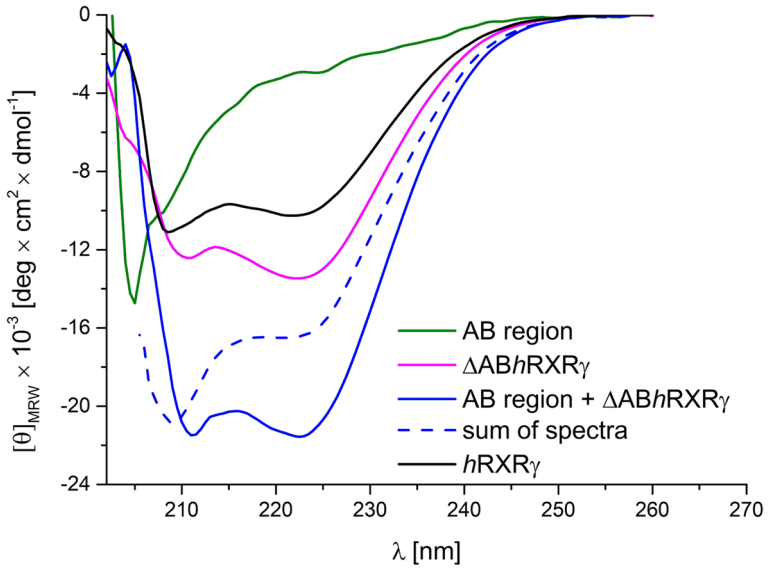

Fig. 9 Far-UV CD spectroscopy reveals the interaction between the AB region of *h*RXRγ and DAB*h*RXRγ. CD spectra of *h*RXRγ, DAB*h*RXRγ, the AB region of *h*RXRγ, mixture of DAB*h*RXRγ and the AB region of *h*RXRγ, and the additive CD spectrum calculated from their individual spectra. All protein samples were prepared at a concentration of 10 µM. The spectra were recorded at 20 °C

showed a predominant α-helical content (44 ± 3.2%), with β-strand, turns, and unordered structures comprising 23 ± 2.2%, 15 ± 1.3%, and 18 ± 2.0%, respectively. In contrast, the calculated additive spectrum indicated higher α-helical (48 ± 2.1%) and unordered content (28 ± 3.7%) but lower β-strand (12 ± 3.0%) and turn (12 ± 2.8%) content.

Taken together, our findings demonstrate that the AB region and ΔAB*h*RXRγ interact, with the nature of this interaction differing between isolated fragments and when they are part of a single polypeptide chain. The intrinsically disordered AB region plays a pivotal role in modulating these interactions, as evidenced by the differences observed in the CD spectrum of full-length *h*RXRγ compared to the additive spectrum of the AB region and ΔAB*h*RXRγ. While interaction occurs, the resulting structure does not fully replicate the native conformation of the intact protein. These results emphasize the importance of protein folding during synthesis in achieving the proper tertiary structure of the full-length receptor.

CD spectra of *h*RXRγ, ΔAB*h*RXRγ, the AB region of *h*RXRγ, mixture of ΔAB*h*RXRγ and the AB region of *h*RXRγ, and the additive CD spectrum calculated from their individual spectra. All protein samples were prepared at a concentration of 10 µM. The spectra were recorded at 20 °C.

To determine the thermodynamic parameter of AB region – ΔAB*h*RXRγ interactions, microscale thermophoresis (MST) was performed (Fig. 10) which can also modulate the transcriptional). MST is a biophysical method for the quantitative characterization of intermolecular interactions in solution [69, 70]. A variation in the fluorescence signal correlates with the binding of a ligand to the fluorescent target thus, MST can be used to determine equilibrium dissociation constants (K_d). The purified recombinant N-terminally 6× His-tagged AB region of *h*RXRγ [33] was first labeled using a His-Tag protein-labeling kit and then mixed with serially diluted ΔAB*h*RXRγ (ligand). AB region of *h*RXRγ showed potential to interact with ΔAB*h*RXRγ, as K_d was estimated to be 11.1 µM ± 5.6.

Thus, MST analysis demonstrated a direct interaction between two fragments of *h*RXRγ – the AB region and ΔAB*h*RXRγ, a result that aligns with the structural arrangement proposed by AlphaFold modeling. As shown by CD analysis, as well as the limited proteolysis and ANS fluorescence experiments presented above, this interaction plays a key role in defining the conformation of the full-length RXR protein.

MST dose–response curve for the labeled 6× His-tagged AB region of *h*RXRγ titrated against ΔAB*h*RXRγ. The resulting curve was fitted to a binding model to determine the K_d. Measurements were performed in triplicate, and error bars represent the standard deviation. MST experiments were conducted using medium MST power and 100% LED power.

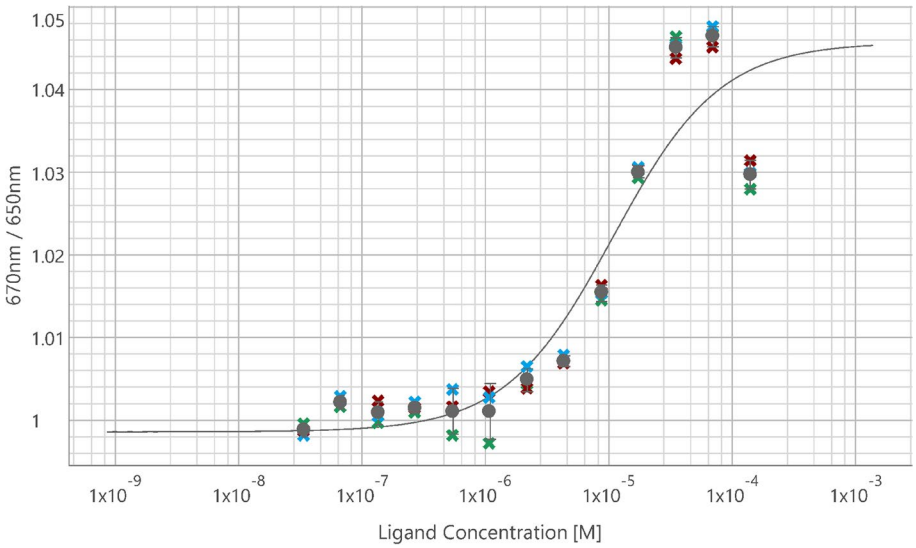

Fig. 10 Interaction between the AB region of *h*RXRγ with DAB*h*RXRγ. MST dose-response curve for the labeled 6×His-tagged AB region of *h*RXRγ titrated against DAB*h*RXRγ. The resulting curve was fitted to a binding model to determine the K_d. Measurements were performed in triplicate, and error bars represent the standard deviation. MST experiments were conducted using medium MST power and 100% LED power

Discussion

The retinoid X receptor (RXR), as common partner for other representatives of the nuclear receptor family, is involved in a diversity of cellular process [17]. However, RXR can also act alone as homodimer or probably by forming higher-order oligomers like homotetramers [18, 71]. Knowledge of the structural features of RXR that mediate oligomer formation and its dynamics is essential for understanding sequence-specific DNA recognition, ligand-binding mechanisms, and their functional outcomes. The crystal structures (of isolated domains or of the multidomain complexes of RXR) [72] indicate that two RXR domains – DBD and LBD – are implicated in governing dimer formation. These two well-ordered globular fragments are flanked by flexible regions – the AB region, the D region and the F region (Fig. 1A), which can also modulate the transcriptional activity of the receptor [73, 74]. The non-conserved AB region of *h*RXRγ plays a crucial role in determining the subtype-, cell type-, and gene-specific functions of RXR. Notably, the unique AB region sequence of each RXR subtype and isoform is a key factor underlying the significant functional differences among RXR variants. The biochemical and biophysical properties of the recombinant isolated AB region of human RXR subtype γ (*h*RXRγ) have been described recently, indicating that the sequence exhibits the structural and functional characteristics of the premolten globule-like (PMG-like) group of intrinsically disordered proteins (IDPs) [33]. However, in the context of the full-length protein, the structural role of the AB region is not understood. To investigate the structural and functional role of the AB region of *h*RXRγ within the context of the full-length RXR, we examined molecular properties of both the full-length *h*RXRγ and a deletion mutant lacking the AB region (ΔAB*h*RXRγ). As an initial step, we determined to what extent the AB region remains disordered within the full-length *h*RXRγ. Both in silico analysis and HDX-MS experiments defined the AB region in *h*RXRγ as intrinsically disordered.

As noted above, RXR functions as a heterodimeric partner for approximately one-third of the members of the human nuclear receptor superfamily. Notably, it can also independently form homodimers and higher-order oligomers such as homotetramers [18, 71]. During purification procedures, both *h*RXRγ and ΔAB*h*RXRγ exhibited a pronounced tendency to oligomerize, a finding further confirmed by chemical cross-linking experiments. Additional experimental approaches, including SEC-MALS and SV-AUC, were employed to assess the ability of *h*RXRγ and ΔAB*h*RXRγ to form higher-order oligomers in solution. These experiments revealed that the intrinsically disordered AB region acts as a structural element that stabilizes higher-order oligomeric states of *h*RXRγ. However, it is important to emphasize that it does not function as a classical stabilizing domain, as seen in well-folded, globular proteins. Crystallographic studies of *h*RXR subtypes, both of isolated domains and multidomain complexes, indicate that dimerization is primarily mediated by DBD and LBD. These structured domains provide the key interfaces responsible for stable dimer formation and can therefore be considered the initial driving force for oligomerization. In contrast, the AB

region is intrinsically disordered and does not oligomerize on its own [33]. Its deletion in ΔAB*h*RXRγ leads to a noticeable reduction in the formation of higher-order oligomeric states. This suggests that the AB region contributes to the stability of these assemblies, possibly through transient interactions that are characteristic of IDRs. Such regions are known to influence protein assembly via dynamic modulation of interdomain interactions and conformational flexibility. This observation leads us to propose, that is not a classical oligomerization interface nor a driving force, it likely stabilizes and fine-tunes the oligomeric behavior of *h*RXRγ.

Our results highlight specific signaling pathways of *h*RXRγ, which contribute to the cell and promoter specificity of receptor action, driven by the presence of the inherently disordered AB region. The variety of higher-order oligomers formed by *h*RXRγ appears to be subtype-specific, as RXRβ does not form such complexes [18], while only homodimers and homotetrames have been observed for RXRα [27]. The propensity of RXR to undergo spontaneous self-assembly in the absence of HREs or ligands does not appear to result in a transcriptionally silent reservoir of the receptor [18, 75]. Instead, the formation of higher-order oligomers provides a broad range of states that RXR can adopt, each offering different regulatory possibilities. These multiple oligomeric variants enable interactions with various proteins, ligands and HREs [27]. The higher-order oligomers of RXR may allow the recognition of DNA sequences that are not recognized by homodimers, thus contributing to subtype-specific promoter utilization. Additionally, the physiological significance of these higher-order oligomers of RXR might relate to the receptor's ability to interact with different ligands.

The presence of the AB region defines the molecular properties of the full-length *h*RXRγ, as demonstrated by its impact on protein stability through CD, ANS fluorescence spectroscopy, and limited proteolysis experiments. *h*RXRγ and ΔAB*h*RXRγ exhibit varying secondary structure content, which changes in response to ionic strength variations from 50 to 300 mM. In *h*RXRγ, a decrease in α-helical content is accompanied by an increase in β-strands, turns, and unordered regions. Conversely, in ΔAB*h*RXRγ, α-helical content increases at the expense of other structural elements. This differential sensitivity of *h*RXRγ and ΔAB*h*RXRγ to ionic strength suggests that the AB region integrates with the rest of the protein, supporting a model in which *h*RXRγ functions as an interrelated entity rather than as a simple assembly of independent regions. The resulting *h*RXRγ conformation likely reflects the AB region's role in modulating the overall structural heterogeneity of the receptor, influencing its molecular properties in a manner that cannot be attributed solely to the properties of its isolated regions. This effect was further demonstrated by the observation that the presence of the AB region in *h*RXRγ modifies the protein's hydrophobicity, leading to reduced stability at elevated temperatures. Structural rearrangements in *h*RXRγ make it less resistant to higher temperatures compared to ΔAB*h*RXRγ, as the transition temperature for *h*RXRγ is at least 10 °C lower than for the deletion mutant. Limited proteolysis also revealed that the AB region, potentially influencing the overall structure of the RXR protein, as certain sites are more accessible in the full-length *h*RXRγ than in ΔAB*h*RXRγ, reflecting differences in the molecular properties of the full-length receptor compared to the deletion mutant. These findings underscore the role of the AB region in modulating the structure and stability of *h*RXRγ.

In many cases, full transcriptional activation by NRs requires a physical intramolecular association between ligand-independent activation function (AF1) located in AB region and ligand-dependent transactivation function (AF2) located in the LBD. This N-terminal/C-terminal interaction has been well-documented for steroid NRs, including the androgen receptor (AR), estrogen receptor (ER) and progesterone receptor (PR) [66, 68, 76]. Interestingly, a similar interaction has also been observed in the non-steroid nuclear receptor Ultraspiracle from *Helicoverpa armigera*, a homolog of mammalian RXR, where it facilitates the formation of scorpion-like structures that stabilize dimers [77]. Recently, the AB region of *h*RXRγ has been shown to promote liquid–liquid phase separation (LLPS) [33, 34] and the formation of AB region liquid condensates significantly influences the rest of the receptor. Specifically, these condensates recruit ΔAB*h*RXRγ into the droplets [34]. Building on these findings, our study used circular dichroism spectroscopy and microscale thermophoresis to demonstrate a direct interaction between the AB region and ΔABhRXRγ, with the K_d estimated at 11.1 μM ± 5.6. While there is currently no direct evidence of full-length *h*RXRγ promoting LLPS in vitro or *in cell*, we propose that LLPS could represent an additional mechanism by which *h*RXRγ function is regulated. This hypothesis warrants further detailed investigation, as intermolecular interactions are likely critical in this process. It appears that both intramolecular and intermolecular interactions play crucial roles in the functions of NRs.

Taken together, our findings provide a cohesive picture of how the intrinsically disordered AB region shapes the structural organization of *h*RXRγ. This region not only modulates the receptor's oligomerization states and

conformational heterogeneity, but also integrates with the structured core domains to define its stability and responsiveness to environmental cues. Overall, this study reveals its critical role as a structural and regulatory element—one that expands the conformational repertoire of *h*RXRγ beyond what is encoded in its folded domains alone.

Conclusions

Our findings offer new insight into the structural complexity of *h*RXRγ and highlight the relevance of disordered regions in nuclear receptor molecular architecture. Comparative analysis of the full-length receptor (*h*RXRγ) and its deletion mutant (ΔAB*h*RXRγ) demonstrated that the AB region is essential for regulating higher-order oligomerization, stability, and conformational heterogeneity. Rather than functioning as an independent unit, the AB region interrelates with the rest of the receptor, fine-tuning its structural flexibility. These findings not only expand our understanding of *h*RXRγ quaternary structure regulation but also underscore the broader significance of disordered regions within nuclear receptors.

Abbreviations

9*c*RA	9-*cis*-Retinoic acid
AF1	Ligand-independent activation function
AF2	Ligand-dependent transactivation function
ANS	8-Anilino-1-naphthalenesulfonic acid
AR	Androgen receptor
ΔAB*h*RXRγ	Deletion mutant of RXR lacking the AB region
CD	Circular dichroism spectroscopy
DBD	DNA-binding domain
DRs	Direct repeats
ER	Estrogen receptor
FXR	Farnesoid X receptor
HDX-MS	Hydrogen-deuterium exchange coupled with mass spectrometry
HRE	Hormone response elements
*h*RXRγ	Human retinoid X receptor γ
IDPs	Intrinsically disordered proteins
IDRs	Intrinsically disordered regions
LBD	Ligand-binding domain
LLPS	Liquid–liquid phase separation
LXR	Liver X receptor
MLOs	Membraneless organelles
MST	Microscale thermophoresis
NRs	Nuclear receptors
PR	Progesterone receptor
PPAR	Peroxisome proliferator-activated receptor
PXR	Pregnane X receptor
RAR	Retinoic acid receptor
RXR	Retinoid X receptor
SEC-MALS	Size-exclusion chromatography with multi-angle light scattering
SV-AUC	Sedimentation velocity analytical ultracentrifugation
TFs	Transcription factors
TR	Thyroid hormone receptor
Usp	Ultraspiracle protein
VDR	Vitamin D receptor

Supplementary Information

The online version contains supplementary material available at https://doi.org/10.1186/s12964-025-02247-3.

Supplementary Material 1.

Acknowledgements

We are grateful to Krzysztof Kobyłecki for his helpful comments regarding the SEC-MALS experiments. We would also like to thank Anna Skorupska-Stasiak for assisting with the HDX-MS experiments. The authors thank the reviewers for helpful comments on the manuscript.

Authors'contributions

KSołtys: Investigation, Methodology, Project administration, Writing—original draft, Writing—review and editing; KSkowronek: Investigation, Methodology, Writing—original draft; DB: Investigation, Methodology, Writing—original draft; KW: Investigation, Methodology, Writing—original draft; AO: Funding acquisition, Supervision, Writing—original draft, Writing—review and editing. The authors read and approved the final manuscript.

Funding

The work was supported by a subsidy from the Polish Ministry of Science and Higher Education for the Faculty of Chemistry of Wrocław University of Science and Technology. The HDX-MS equipment used was sponsored by the Centre for Preclinical Research and Technology (CePT), a project cosponsored by the European Regional Development Fund and Innovative Economy, and The National Cohesion Strategy of Poland. IIMCB core facilities (IN-MOL-CELL infrastructure) were funded by the European Union and co-financed under the European Funds for Smart Economy 2021–2027 (FENG).
Polish Ministry of Science and Higher Education

Data availability

No datasets were generated or analysed during the current study.

Declarations

Ethics approval and consent to participate

Not applicable.

Consent for publication

Not applicable.

Competing interests

The authors declare no competing interests.

Received: 7 February 2025 Accepted: 12 May 2025
Published online: 26 May 2025

References

1. Habchi J, Tompa P, Longhi S, Uversky VN. Introducing protein intrinsic disorder. Chem Rev United States. 2014;114:6561–88.
2. Bondos SE, Dunker AK, Uversky VN. Intrinsically disordered proteins play diverse roles in cell signaling. Cell Commun Signal. England; 2022;20:20.
3. Uversky VN. Intrinsically Disordered Proteins and Their "Mysterious" (Meta) Physics. Front Phys. 2019;7:10. https://doi.org/10.3389/fphy.2019.00010.
4. Moses D, Ginell GM, Holehouse AS, Sukenik S. Intrinsically disordered regions are poised to act as sensors of cellular chemistry. Trends Biochem Sci England. 2023;48:1019–34.
5. Oldfield CJ, Dunker AK. Intrinsically disordered proteins and intrinsically disordered protein regions. Annu Rev Biochem. 2014;83:553–84. https://doi.org/10.1146/annurev-biochem-072711-164947.
6. Chakrabarti P, Chakravarty D. Intrinsically disordered proteins/regions and insight into their biomolecular interactions. Biophys Chem. 2022;283: 106769.
7. Darling AL, Liu Y, Oldfield CJ, Uversky VN. Intrinsically Disordered Proteome of Human Membrane-Less Organelles. Proteomics Germany. 2018;18:e1700193.
8. Uversky VN, Kuznetsova IM, Turoverov KK, Zaslavsky B. Intrinsically disordered proteins as crucial constituents of cellular aqueous two phase systems and coacervates. FEBS Lett England. 2015;589:15–22.
9. Bah A, Forman-Kay JD. Modulation of Intrinsically Disordered Protein Function by Post-translational Modifications. J Biol Chem. 2016;291:6696–705.
10. He B, Wang K, Liu Y, Xue B, Uversky VN, Dunker AK. Predicting intrinsic disorder in proteins: an overview. Cell Res England. 2009;19:929–49.

11. Liu J, Perumal NB, Oldfield CJ, Su EW, Uversky VN, Dunker AK. Intrinsic Disorder in Transcription Factors. Biochemistry American Chemical Society. 2006;45:6873–88.
12. Fuxreiter M, Tompa P, Simon I, Uversky VN, Hansen JC, Asturias FJ. Malleable machines take shape in eukaryotic transcriptional regulation. Nat Chem Biol United States. 2008;4:728–37.
13. Tsafou K, Tiwari PB, Forman-Kay JD, Metallo SJ, Toretsky JA. Targeting Intrinsically Disordered Transcription Factors: Changing the Paradigm. J Mol Biol. 2018;430:2321–41.
14. Shammas SL. Mechanistic roles of protein disorder within transcription. Curr Opin Struct Biol. 2017;42:155–61.
15. Sammak S, Zinzalla G. Targeting protein–protein interactions (PPIs) of transcription factors: Challenges of intrinsically disordered proteins (IDPs) and regions (IDRs). Prog Biophys Mol Biol. 2015;119:41–6.
16. Szanto A, Narkar V, Shen Q, Uray IP, Davies PJA, Nagy L. Retinoid X receptors: X-ploring their (patho)physiological functions. Cell Death Differ England. 2004;11(Suppl 2):S126-43.
17. Lefebvre P, Benomar Y, Staels B. Retinoid X receptors: common heterodimerization partners with distinct functions. Trends Endocrinol Metab. 2010;21:676–83.
18. Chen H, Privalsky ML. Cooperative formation of high-order oligomers by retinoid X receptors: an unexpected mode of DNA recognition. Proc Natl Acad Sci U S A. 1995;92:422–6.
19. Zhao L, Zhou S, Gustafsson J-Å. Nuclear Receptors: Recent Drug Discovery for Cancer Therapies. Endocr Rev. 2019;40:1207–49.
20. Schulman IG. Nuclear receptors as drug targets for metabolic disease. Adv Drug Deliv Rev. 2010;62:1307–15.
21. Pawlak M, Lefebvre P, Staels B. General molecular biology and architecture of nuclear receptors. Curr Top Med Chem. 2012;12:486–504.
22. Rastinejad F. Retinoid X receptor and its partners in the nuclear receptor family. Curr Opin Struct Biol England. 2001;11:33–8.
23. Osz J, McEwen AG, Poussin-Courmontagne P, Moutier E, Birck C, Davidson I, et al. Structural basis of natural promoter recognition by the retinoid X nuclear receptor. Sci Rep England. 2015;5:8216.
24. Orlov I, Rochel N, Moras D, Klaholz BP. Structure of the full human RXR/VDR nuclear receptor heterodimer complex with its DR3 target DNA. EMBO J. 2012;31:291–300.
25. Gampe RTJ, Montana VG, Lambert MH, Wisely GB, Milburn MV, Xu HE. Structural basis for autorepression of retinoid X receptor by tetramer formation and the AF-2 helix. Genes Dev United States. 2000;14:2229–41.
26. Kersten S, Dong D, Lee Wy, Reczek PR, Noy N. Auto-silencing by the retinoid X receptor. J Mol Biol Netherlands. 1998;284:21–32.
27. Kersten S, Kelleher D, Chambon P, Gronemeyer H, Noy N. Retinoid X receptor alpha forms tetramers in solution. Proc Natl Acad Sci U S A United States. 1995;92:8645–9.
28. Yasmin R, Yeung KT, Chung RH, Gaczynska ME, Osmulski PA, Noy N. DNA-looping by RXR tetramers permits transcriptional regulation "at a distance." J Mol Biol England. 2004;343:327–38.
29. Chen ZP, Iyer J, Bourguet W, Held P, Mioskowski C, Lebeau L, et al. Ligand- and DNA-induced dissociation of RXR tetramers. J Mol Biol Netherlands. 1998;275:55–65.
30. Egea PF, Rochel N, Birck C, Vachette P, Timmins PA, Moras D. Effects of ligand binding on the association properties and conformation in solution of retinoic acid receptors RXR and RAR. J Mol Biol Netherlands. 2001;307:557–76.
31. Mangelsdorf DJ, Borgmeyer U, Heyman RA, Zhou JY, Ong ES, Oro AE, et al. Characterization of three RXR genes that mediate the action of 9-cis retinoic acid. Genes Dev United States. 1992;6:329–44.
32. Lavery DN, Mcewan IJ. Structure and function of steroid receptor AF1 transactivation domains: induction of active conformations. Biochem J. 2005;391:449–64.
33. Sołtys K, Ożyhar A. Ordered structure-forming properties of the intrinsically disordered AB region of hRXRγ and its ability to promote liquid-liquid phase separation. J Steroid Biochem Mol Biol. 2020;198: 105571.
34. Sołtys K, Wycisk K, Ożyhar A. Liquid-liquid phase separation of the intrinsically disordered AB region of hRXRγ is driven by hydrophobic interactions. Int J Biol Macromol Netherlands. 2021;183:936–49.
35. Butt TR, Edavettal SC, Hall JP, Mattern MR. SUMO fusion technology for difficult-to-express proteins. Protein Expr Purif. 2005;43:1–9.
36. Studier FW. Protein production by auto-induction in high density shaking cultures. Protein Expr Purif United States. 2005;41:207–34.
37. Weeks SD, Drinker M, Loll PJ. Ligation independent cloning vectors for expression of SUMO fusions. Protein Expr Purif. 2007;53:40–50.
38. Gill SC, von Hippel PH. Calculation of protein extinction coefficients from amino acid sequence data. Anal Biochem. 1989;182:319–26.
39. Laemmli UK. Cleavage of Structural Proteins during the Assembly of the Head of Bacteriophage T4. Nature. 1970;227:680–5.
40. Weber K, Pringle JR, Osborn M. Measurement of molecular weights by electrophoresis on SDS-acrylamide gel. Methods Enzymol; 1972. p. 3–27. https://doi.org/10.1016/s0076-6879(72)26003-7. PMID: 4680711.
41. Schuck P, Perugini MA, Gonzales NR, Howlett GJ, Schubert D. Size-distribution analysis of proteins by analytical ultracentrifugation: strategies and application to model systems. Biophys J. 2002;82:1096–111.
42. Schuck P. Size-distribution analysis of macromolecules by sedimentation velocity ultracentrifugation and lamm equation modeling. Biophys J. 2000;78:1606–19.
43. Lebowitz J, Lewis MS, Schuck P. Modern analytical ultracentrifugation in protein science: a tutorial review. Protein Sci. 2002;11:2067–79.
44. Sreerama N, Woody RW. Computation and analysis of protein circular dichroism spectra. Methods Enzymol United States. 2004;383:318–51.
45. Ferguson RN, Edelhoch H, Saroff HA, Robbins J, Cahnmann HJ. Negative cooperativity in the binding of thyroxine to human serum prealbumin. Preparation of tritium-labeled 8-anilino-1-naphthalenesulfonic acid. Biochemistry United States. 1975;14:282–9.
46. Gasteiger E, Hoogland C, Gattiker A, Duvaud S, Wilkins MR, Appel RD, et al. Protein Identification and Analysis Tools on the ExPASy Server. In: Walker JM, editor., et al., Proteomics Protoc Handb. Humana Press; 2005. p. 571–607.
47. Mészáros B, Erdös G, Dosztányi Z. IUPred2A: Context-dependent prediction of protein disorder as a function of redox state and protein binding. Nucleic Acids Res. 2018;46:W329–37.
48. Erdős G, Dosztányi Z. Analyzing Protein Disorder with IUPred2A. Curr Protoc Bioinforma United States. 2020;70:e99.
49. Kozlowski LP, Bujnicki JM. MetaDisorder: a meta-server for the prediction of intrinsic disorder in proteins. BMC Bioinformatics England. 2012;13:111.
50. Cilia E, Pancsa R, Tompa P, Lenaerts T, Vranken WF. From protein sequence to dynamics and disorder with DynaMine. Nat Commun England. 2013;4:2741.
51. Cilia E, Pancsa R, Tompa P, Lenaerts T, Vranken WF. The DynaMine webserver: predicting protein dynamics from sequence. Nucleic Acids Res. 2014;42:W264–70.
52. Abramson J, Adler J, Dunger J, Evans R, Green T, Pritzel A, et al. Accurate structure prediction of biomolecular interactions with AlphaFold 3. Nature England. 2024;630:493–500.
53. Meng EC, Goddard TD, Pettersen EF, Couch GS, Pearson ZJ, Morris JH, et al. UCSF ChimeraX: Tools for structure building and analysis. Protein Sci United States. 2023;32:e4792.
54. Chalmers MJ, Busby SA, Pascal BD, Southern MR, Griffin PR. A two-stage differential hydrogen deuterium exchange method for the rapid characterization of protein/ligand interactions. J Biomol Tech United States. 2007;18:194–204.
55. Some D, Amartely H, Tsadok A, Lebendiker M. Characterization of Proteins by Size-Exclusion Chromatography Coupled to Multi-Angle Light Scattering (SEC-MALS). J Vis Exp. 2019;(148). https://doi.org/10.3791/59615. PMID: 31282880.
56. Chaturvedi SK, Ma J, Zhao H, Schuck P. Use of fluorescence-detected sedimentation velocity to study high-affinity protein interactions. Nat Protoc England. 2017;12:1777–91.
57. Tcherkasskaya O, Uversky VN. Denatured collapsed states in protein folding: example of apomyoglobin. Proteins United States. 2001;44:244–54.
58. Uversky VN. What does it mean to be natively unfolded? Eur J Biochem. 2002;269:2–12.
59. Greenfield NJ. Using circular dichroism collected as a function of temperature to determine the thermodynamics of protein unfolding and binding interactions. Nat Protoc England. 2006;1:2527–35.
60. Kelly SM, Price NC. The use of circular dichroism in the investigation of protein structure and function. Curr Protein Pept Sci United Arab Emirates. 2000;1:349–84.
61. Kelly SM, Jess TJ, Price NC. How to study proteins by circular dichroism. Biochim Biophys Acta - Proteins Proteomics. 2005;1751:119–39.
62. Stryer L. The interaction of a naphthalene dye with apomyoglobin and apohemoglobin: A fluorescent probe of non-polar binding sites. J Mol Biol. 1965;13:482–95.

63. Van den Burg B, Dijkstra BW, Vriend G, Van der Vinne B, Venema G, Eijsink VG. Protein stabilization by hydrophobic interactions at the surface. Eur J Biochem England. 1994;220:981–5.
64. Desantis F, Miotto M, Di Rienzo L, Milanetti E, Ruocco G. Spatial organization of hydrophobic and charged residues affects protein thermal stability and binding affinity. Sci Rep England. 2022;12:12087.
65. Drapeau GR, Boily Y, Houmard J. Purification and properties of an extracellular protease of Staphylococcus aureus. J Biol Chem United States. 1972;247:6720–6.
66. Ikonen T, Palvimo JJ, Jänne OA. Interaction between the amino- and carboxyl-terminal regions of the rat androgen receptor modulates transcriptional activity and is influenced by nuclear receptor coactivators. J Biol Chem United States. 1997;272:29821–8.
67. Métivier R, Penot G, Flouriot G, Pakdel F. Synergism between ERalpha transactivation function 1 (AF-1) and AF-2 mediated by steroid receptor coactivator protein-1: requirement for the AF-1 alpha-helical core and for a direct interaction between the N- and C-terminal domains. Mol Endocrinol United States. 2001;15:1953–70.
68. Dong X, Challis JRG, Lye SJ. Intramolecular interactions between the AF3 domain and the C-terminus of the human progesterone receptor are mediated through two LXXLL motifs. J Mol Endocrinol England. 2004;32:843–57.
69. Jerabek-Willemsen M, André T, Wanner R, Roth HM, Duhr S, Baaske P, et al. MicroScale Thermophoresis: Interaction analysis and beyond. J Mol Struct. 2014;1077:101–13.
70. Seidel SAI, Dijkman PM, Lea WA, van den Bogaart G, Jerabek-Willemsen M, Lazic A, et al. Microscale thermophoresis quantifies biomolecular interactions under previously challenging conditions. Methods United States. 2013;59:301–15.
71. Lin BC, Wong CW, Chen HW, Privalsky ML. Plasticity of tetramer formation by retinoid X receptors. An alternative paradigm for DNA recognition. J Biol Chem United States. 1997;272:9860–7.
72. Dawson MI, Xia Z. The retinoid X receptors and their ligands. Biochim Biophys Acta. 2012;1821:21–56.
73. Staller M V, Ramirez E, Kotha SR, Holehouse AS, Pappu R V, Cohen BA. Directed mutational scanning reveals a balance between acidic and hydrophobic residues in strong human activation domains. Cell Syst [Internet]. 2022;13:334–345.e5. Available from: https://www.sciencedirect.com/science/article/pii/S2405471222000023
74. Ravarani CN, Erkina TY, De Baets G, Dudman DC, Erkine AM, Babu MM. High-throughput discovery of functional disordered regions: investigation of transactivation domains. Mol Syst Biol Germany. 2018;14:e8190.
75. Kersten S, Gronemeyer H, Noy N. The DNA Binding Pattern of the Retinoid X Receptor Is Regulated by Ligand-dependent Modulation of Its Oligomeric State*. J Biol Chem [Internet]. 1997;272:12771–7. Available from: https://www.sciencedirect.com/science/article/pii/S0021925818404796
76. Benecke A, Chambon P, Gronemeyer H. Synergy between estrogen receptor alpha activation functions AF1 and AF2 mediated by transcription intermediary factor TIF2. EMBO Rep England. 2000;1:151–7.
77. Wycisk K, Tarczewska A, Kaus-Drobek M, Dadlez M, Hołubowicz R, Pietras Z, et al. Intrinsically disordered N-terminal domain of the Helicoverpa armigera Ultraspiracle stabilizes the dimeric form via a scorpion-like structure. J Steroid Biochem Mol Biol England. 2018;183:167–83.

Publisher's Note